- 1 Investigating Preservation of Stable Isotope Ratios in Subfossil Deep-Sea Proteinaceous
- 2 Coral Skeletons as Paleo-Recorders of Biogeochemical Information over Multimillennial
- 3 Timescales
- 4 Danielle S. Glynn, UC Santa Cruz, CA, USA. Corresponding Author Email: dglynn@ucsc.edu
- 5 Kelton McMahon, University of Rhode Island, RI, USA. Email: kelton mcmahon@uri.edu
- 6 Owen Sherwood, Dalhousie University, Halifax, NS, Canada. Email: owen.sherwood@dal.ca
- 7 Thomas P. Guilderson, UC Santa Cruz, CA, USA. Email: tguilder@ucsc.edu
- 8 Matthew D. McCarthy, UC Santa Cruz, CA, USA. Email: mdmccar@ucsc.edu

9 Abstract:

10

11

12

13

14

15

16

17

18

19

20

21

22

23

24

25

26

27

28

29

Paleoproxy records in deep-sea proteinaceous coral skeletons can reconstruct past ocean conditions on centennial to millennial time scales. Commonly recovered subfossil specimens could potentially extend these archives through the Holocene. However, protein matrix stability and integrity of stable isotope proxies over multi-millennial timescales in such specimens have never been examined. Here we compare amino acid (AA) composition together with bulk and AA compound-specific carbon (δ^{13} C) and nitrogen (δ^{15} N) isotopes in live-collected and subfossil (~9.6-11.6 kyrs BP) Kulamanamana haumeaae deep-sea coral specimens from the central Pacific to understand the effects of long-duration benthic oxic exposure on primary coral chemistry. We find large coupled shifts in bulk $\delta^{15}N$ (~7‰) and $\delta^{13}C$ (~2‰) in the outermost portion (0-10 mm) of the subfossil coral, coincident with extensive alteration of the protein matrix. Microstructural changes in skeletal texture coincide with higher C/N ratios (+0.8) and isotope-based amino acid degradation parameters (e.g. $\Sigma V \ge 3$), indicating extensive degradation of seawater-exposed gorgonin. However, interior gorgonin (>10 mm) retained amino acid molecular compositions (with exception of major Glycine loss) and bulk and amino acid-specific isotopic values that were similar to live-collected specimens. These results indicate that compound-specific isotope analysis of amino acids can reconstruct paleo-oceanographic biogeochemical and ecosystem information in subfossil corals beyond a clear diagenetic horizon, which is easily identifiable from an evaluation of C/N ratios together with the ΣV degradation proxy.

1. Introduction

30

31

32

33

34

35

36

37

38

39

40

41

42

43

44

45

46

47

48

49

50

51

52

Deep-sea proteinaceous corals are ideal recorders of sub-decadal resolution surface biogeochemistry, due to their ubiquitous distribution, long lifespans, and near continuous deposition of skeletal material (reviewed in Williams 2020). These corals consume organic matter exported from the surface ocean and incorporate the isotopic values of exported production into concentric growth layers in their proteinaceous skeletons (Druffel et al., 1995; Roark et al., 2006). In recent years, deep-sea proteinaceous coral skeletons have been used to reconstruct the history of exported organic matter over centennial to millennial timescales globally, including the North Pacific Gyre (Sherwood et al., 2014; McMahon et al., 2015; Glynn et al., 2019), North Atlantic (Sherwood et al. 2009a, 2011), southern Australia (Sherwood et al., 2009b), the Equatorial Pacific (Williams and Grottoli, 2010), and the California Margin (Hill et al., 2014; Schiff et al., 2014). Deep-sea proteinaceous coral studies have been particularly useful in understanding the most recent millennia of ocean history, a period characterized by rapid oceanographic and climatic change, but one in which detailed sedimentary records in many locations are severely limited by slow sedimentation rates or significant bioturbation. In many regions, proteinaceous corals also represent the only archive capable of decadal or finer temporal scale reconstructions, making them especially useful to understand multi-decadal variability of biogeochemical cycling and phytoplankton community dynamics recorded in the signal of export production (Sherwood et al., 2011; 2014, McMahon et al., 2015).

To properly evaluate paleo-environmental interpretations from organic proxies, the preservation of chemical and isotopic information must be carefully considered. Proteinaceous deep-sea coral skeletons are composed of a cross-linked, fibrillar protein that is among the most diagenetically resistant proteinaceous materials known (Goldberg, 1974, 1976; Ehrlich, 2010;

Strzepek et al., 2014). For example, skeletons of black corals are predominantly composed of protein (~50-70%) and contain lipids, diphenols, and chitin (Holl et al. 1992). However, far less is known for gold corals besides being composed of primarily amino acids (AAs) (Goodfriend 1997, Sherwood et al. 2006, 2014). At the molecular level, the AA composition of modern *K. haumeaae* shows little variability over the duration of the coral skeleton's growth (Goodfriend, 1997; Sherwood et al., 2006), and AA composition is also similar in live-collected versus 1000-2000 year old specimens (Sherwood et al., 2006), suggesting that coral skeleton protein is stable over at least millennial time frames.

53

54

55

56

57

58

59

60

61

62

63

64

65

66

67

68

69

70

71

72

73

74

75

The abundance of non-living coral skeletons encountered on the seafloor in many locations suggests the possibility to go far beyond the time horizon constrained by living corals. For example, Guilderson and coauthors (2013) describe a range of ¹⁴C dated specimens from both the Hawaiian and Line Islands that collectively spanned the entire Holocene. Edinger and Sherwood (2012) conducted year-long decay experiments on deep-sea corals of different skeletal compositions and documented a range of physical changes such as pitting, corrosion, hydration, and disintegration of the organic gorgonin. Noé and Dullo (2006) and Noé et al. (2007) noted the presence of micritized borings in subfossil gorgonian corals. To date, there have been no detailed studies of $\delta^{15}N$ and $\delta^{13}C$ preservation of subfossil deep-sea proteinaceous coral specimens collected in-situ on the seafloor. Thus, the susceptibility of the gorgonin protein matrix to degradation and the integrity of archived geochemical information on multi-millennial timescales are not well known. A detailed understanding of skeletal preservation over long timescales will substantially improve confidence in the use of subfossil corals for paleoceanographic study, since degradative effects could easily be confused with signatures of past environmental variation.

The goal of this study was to assess the integrity of the $\delta^{15}N$ and $\delta^{13}C$ values and AA profiles recorded in deep-sea proteinaceous corals over extensive time and degradation potential. We compared the structural, chemical, and isotopic data in a subfossil (~9.6-11.6 kyr BP) coral with the same properties in a live-collected specimen from the same location at Cross Seamount, Hawaii. We used a multi-metric approach to examine central aspects of physical, chemical, and isotopic change as a function of preservation along a gradient from inner protected layers to outer seawater exposed regions. Scanning electron microscopy (SEM) was used to investigate physical structural change in the skeleton matrix. Chemical composition changes were examined using bulk tissue carbon to nitrogen (C/N) elemental ratios and molecular-level AA composition (mol%). Patterns in bulk tissue $\delta^{15}N$ and $\delta^{13}C$ values as well as carbon and nitrogen compoundspecific isotope analysis of AAs (CSIA-AA) were compared to examine potential impacts of degradation on geochemical fidelity. These comparisons allowed us to directly determine how ~10 kyrs of oxic seawater exposure altered the chemistry and the paleo-archival potential of the proteinaceous skeleton. We used these data to propose metrics for evaluating the integrity of proteinaceous corals and the geochemical data they archive.

2. Materials and Methods

76

77

78

79

80

81

82

83

84

85

86

87

88

89

90

91

92

93

94

95

96

97

98

2.1 Study site and sample collection

Living and subfossil deep-sea proteinaceous corals (*Kulamanamana haumaeae*) were collected from 447 and 415 m respectively from Cross Seamount (19°N, 158°W), southwest of the Big Island of Hawaii, in 2004. Cross Seamount waters at 400 m have average in situ temperatures of ~9 °C and dissolved oxygen concentration of ~100-120 μmol/kg (Boyer et al., 2018). The polyps of live-collected corals were removed and all skeletons were rinsed first with seawater, followed by freshwater, before being air dried on deck. In the lab, ~0.7 cm thick cross-

sectional disks were sectioned from near the base of each skeleton, then polished and mounted to glass slides, following standard procedures (Sherwood et al., 2014). A detailed sample processing flow chart and description can be found in the supplemental file (Fig. S1A).

2.2 Scanning electron microscopy (SEM)

For scanning electron microscope images, sections of the same coral disks were coated with ~20 nm of gold using a Technics Hummer VI sputter coater (3 minutes @ 80 mtorr, 17 mA current) and then imaged on a FEI Quanta 3D dual beam microscope (electron beam operating at 5 kV and 6.7 pA) in the W.M. Keck Center for Nanoscale Optofluidics at the University of California – Santa Cruz. SEM images (300 μm and 30-40 μm resolution) were visually compared to examine structural changes in the skeletal matrix between the live-collected and subfossil corals.

2.3 Radiocarbon dating and age models

Radiocarbon dating was performed on nine sample aliquots (~1 mg total material) each spread ~5 mm apart along the skeleton cross section transect. Samples were first fumed with concentrated HCl and subsequently dried before being transferred with methanol into 6 mm short quartz tubes and dried. The 6 mm tubes were then placed inside larger 9 mm quartz tubes with an appropriate amount of CuO, prior to pumping off excess atmosphere, sealing, and combusting to produce CO₂. The CO₂ after cryogenic purification was converted to graphite and analyzed at the Lawrence Livermore National Laboratory. Results were corrected for δ^{13} C and background 14 C using similarly handled 14 C-free coal. Radiocarbon results were transformed into calibrated years before present (yr BP). These ages and subsequent age models were generated with Calib 8.2 (Stuiver et al. 2021) using a local reservoir (Δ R) correction of -177 ± 16, (Druffel et al., 2001;

Guilderson et al., 2021) and the Marine20 database (Heaton et al. 2020) and linearly interpreted to provide a continuous age-model.

2.4 Bulk stable isotope analysis

121

122

123

124

125

126

127

128

129

130

131

132

133

134

135

136

137

138

139

140

141

142

143

A computerized Merchanteck micromill was used to drill a radial transect from the outside to the inner layers of the coral skeleton cross section at 0.1 mm resolution, yielding 2-3 mg of powdered skeletal material per sample interval. All 168 samples from the live-collected coral were analyzed (155 samples in duplicate); while of the 455 subfossil samples drilled, 193 were analyzed, with a greater sample density analyzed from the outermost 10 mm. Bulk powdered coral material (~0.4 mg) was enclosed in tin capsules for bulk δ^{13} C and δ^{15} N analyses via continuous-flow isotope-ratio mass spectrometry (IRMS) using a Carlo-Erba elemental analyzer connected to an Optima Isotope Ratio Mass Spectrometer (IRMS). C/N ratios were simultaneously determined. The analytical error for these measurements, as determined from analysis of standards of known composition (pugel and acetanilide), was $\pm 0.2\%$ for both δ^{13} C and δ^{15} N values and ± 0.1 for C/N ratios. To test for the impact of secondary authigenic carbonate in the sample matrix, a subset of the same samples from the subfossil coral (1–2 mg each, n = 7) were acidified using 1 N HCl for 20 h under refrigerated conditions, followed by filtration onto a 0.22 µm glass fiber filter. The filter was dried overnight at 45°C before material was transferred into a tin capsule and analyzed following the same procedure as described above.

2.5 Amino Acid Molar Percent

Adjacent growth bands were combined to obtain ~10-11 mg of total material which, after homogenization, was used for each analysis (typically used 8-10 samples of ~1 mg from each adjacent 0.1 mm layers). Of these composite samples, approximately 0.5-1 mg of coral material was needed for measurement of AA molar concentrations, with the rest being used for CSIA-AA

described in Section 2.6. Wet chemical protocols for AA measurements in proteinaceous corals followed established protocols (detailed in McMahon et al, 2018). Briefly, individual AAs were liberated using standard acid hydrolysis conditions (1 ml of 6 N HCl at 110°C for 20 h), then spiked with a norleucine internal standard and derivitized, followed by purification with cation-exchange chromatography and a salt-removal step (p-buffer = KH₂PO₄ + Na₂HPO₄ in Milli-Q water, pH 7), and finally rinsed with chloroform three times with centrifugation before final conversion to trifluoroacetyl/isopropyl ester (TFAA) derivatives. The AA mole percent (mol%) compositions were quantified using a GC–MS (Agilent 7890 GC coupled to a 5975 MSD) based on single ion monitoring data of the major ion relative to authentic AA external standard calibration curves. Commercial AA standards (Pierce Biochemicals) were used to create concentration series, and response factors from these external standards were used to calculate relative molar concentrations. Reproducibility, as measured by the standard deviation of GC-MS replicates analyses, typically averaged <5 mol%.

2.6 Compound Specific Stable Isotope Analysis of Amino Acids (CSIA-AA)

CSIA-AA for both carbon and nitrogen was performed on aliquots of the same TFAA derivatives prepared as described in Section 2.5, using ~4 mg for δ^{13} C and ~6 mg δ^{15} N CSIA-AA measurements. Derivatized samples were injected in triplicate on a coupled Gas Chromatography- IRMS (Thermo Trace GC, coupled to a Delta + IRMS), as described in McMahon et al. (2018). Isotopic ratios were measured for 13 of the common protein AAs (see supplementary material, Fig. S1): alanine (Ala), glycine (Gly), serine (Ser), valine (Val), threonine (Thr), leucine (Leu), isoleucine (Ile), proline (Pro), phenylalanine (Phe), tyrosine (Tyr), lysine (Lys), glutamine + glutamic acid (Glx), and asparagine + aspartic acid (Asx). Cystine (Cys) and histidine (His) break down during acid hydrolysis and were not measured.

For $\delta^{13}C_{AA}$ higher sensitivity coupled with good chromatographic separation permitted all AA $\delta^{13}C$ values to be measured in single chromatographic run (Fig. S1). However for $\delta^{15}N_{AA}$, the much larger on-column AA amounts required by much lower intrinsic IRMS sensitivity for N made it impossible to obtain both adequate chromatography and peaks sizes simultaneously for all AAs in a single run. We therefore performed independent GC-IRMS $\delta^{15}N$ run series for high verses low mol% AAs (Fig. S1). The early eluting AA peaks (Ala, Gly, Ser, Thr, and Val) were all large and well separated (Fig. S1), and necessitated only duplicate injections. GC-IRMS error was therefore reported for these peaks as mean deviations. Subsequent independent runs at higher concentrations then employed a cut-off method to remove early peaks (directed to backflush), so that lower mol% peaks could be quantified (Asx, Glx, Ile, Leu, Lys, Phe, Pro, Tyr). These injections were made in triplicate, with concentrations adjusted to produce at least 80 mV IRMS N₂ signal intensity for the smallest peaks (typically Phe and Ile).

Overall reproducibility for individual AA isotopes values among sample injections was <1‰ for both δ^{13} C and δ^{15} N CSIA-AA, based on internal lab working standards. Accuracy of δ^{13} C and δ^{15} N CSIA-AA data was verified following protocols described in McCarthy et al., 2013. Briefly, three independent, overlapping approaches were used to assess accuracy: first a Nor-Leu internal standard added to every sample, second an external (L-amino acid) AA standard mix injected repeatedly after every third sample, and finally a natural cyanobacteria long term (> 10 yr) in-house working standard, run as an unknown with every sample batch. The Nor-Leu internal standard was used to verify that each specific injection for each sample gave expected values. The external bracketed standards were used in different ways for δ^{13} C and δ^{15} N values based on the need to correct for added derivatization moieties for δ^{13} C only. For δ^{13} C, the measured IRMS values are not actual AA δ^{13} C values but must corrected for added derivative C;

this was done following the method of Silfer (1991). For $\delta^{15}N$ values the measured IRMS values directly represent the $\delta^{15}N$ value of each AA and therefore external standard values can be used to directly assess accuracy and make corrections. For $\delta^{15}N$, the average measured $\delta^{15}N$ value of each external standard AA across the entire run was therefore compared against its authentic value, and any systematic bias/offset used to correct sample AA values, following the approach described by McCarthy et al., 2013 (supplementary information, Fig. S2). Finally, both $\delta^{13}C$ and $\delta^{15}N$ AA results from the McCarthy lab internal laboratory reference material (dried/homogenized cyanobacteria) standard run with each sample batch were evaluated for accuracy against a long term (>10 yr) internal control chart. The supplemental file contains more information on the order of sample processing, including specific protocols for CSIA-AA corrections, representative chromatograms, and minimum mV peak information (Fig. S1A, S1B).

2.7 Nomenclature, AA groupings, and CSIA-AA parameters

We report and discuss AA isotope data in terms of commonly used CSIA-AA groupings for both δ^{13} C and δ^{15} N, which in turn are based on metabolic pathways and observed differences in isotope fractionation during trophic transfer (reviewed by McMahon and McCarthy, 2016, Ohkouchi et al., 2017). For δ^{15} N data, we treat Phe, Tyr, and Lys as Source AAs (those with minimal isotope fractionation during trophic transfer); Asx, Glx, Ile, Leu, Pro, Val as Trophic AAs (close linkage to central glutamate pool, with correspondingly large isotope fractionation during trophic transfer), and Gly and Ser as Intermediate AAs, based on recent literature that shows they display variable behavior, very often falling between the two customary groupings (McMahon and McCarthy, 2016). Lastly, Thr was plotted alone, as it displays a unique inverse isotope fractionation behavior with trophic transfer (McMahon and McCarthy, 2016).

For δ^{13} C, we used common essential and non-essential AAs categories. There is minimal isotope fractionation for essential AAs with trophic transfer, while there can be highly variable fractionation in the nonessential AAs due to resynthesis (McMahon et al. 2010). The essential AAs (Thr, Ile, Val, Phe, and Leu) can be synthesized by both phytoplankton and microbes, however most metazoans cannot synthesize them and must incorporate the essential AA from their diet (Larsen et al. 2013). While we note that it is possible that some coral species, or more likely microbes associated with them, could also potentially synthesize essential AA, prior work has indicated that essential AA δ^{13} C CSIA-AA in proteinaceous corals correspond to expected primary production patterns and local endmember values and thus directly track export production (Schiff et al., 2014, McMahon et al., 2018, Shen et al., 2021).

We quantified possible microbial reworking of skeletal protein using AA $\delta^{15}N$ values using the CSIA-AA metric ΣV , which is a proxy for total heterotrophic microbial AA resynthesis of proteinaceous material (McCarthy et al., 2007, Ohkouchi et al, 2017). ΣV was calculated using the average deviation of $\delta^{15}N$ values of the trophic AAs Ala, Val, Leu, Ile, Pro, Asx, Glx:

$$\sum V = \frac{1}{n} \sum |X_i|$$

where X_i is the offset in $\delta^{15}N$ of each individual AA from the average ($X_i = \delta^{15}N_i - AVG \delta^{15}N_i$), and n is the number of AAs used in the calculation.

The CSIA-AA-based trophic position (TP_{CSIA-AA Skeleton}) of deep-sea corals is a proxy for trophic structure of both the coral and the overlying planktonic food web contributing to export production. This parameter was calculated using the difference in Phe (source) and Glx (trophic) δ^{15} N values according to a proteinaceous coral – specific formula:

$$TP_{CSIA-AA\,Skeleton} = 1 + \left(\frac{\delta^{15}N_{Glx} + \partial - \delta^{15}N_{Phe} - \beta}{TDF_{Glx-Phe}}\right)$$

recently determined by McMahon et al. (2018). This formula incorporates an additional correction factor (∂) for Glx of 3.4 ± 0.1‰ to account for the consistent offsets observed between polyp and skeletal Glx δ^{15} N values across multiple deep-sea coral species (McMahon et al., 2018). The β value (3.4‰; empirical difference between the δ^{15} N_{Glx} and δ^{15} N_{Phe} of non-vascular autotrophs) and the TDF value (7.6‰; trophic discrimination factor of δ^{15} N_{Glx} relative to δ^{15} N_{Phe} per trophic transfer; Chikaraishi et al., 2009). We note that alternate β (3.3 ± 1.8‰; Ramirez et al. 2021) and TDF (6.6 ± 1.7‰; Nielson et al. 2015) values have recently been proposed to represent better averages over many ecosystems. We present alternate TP value using these values in the supplemental material, however because the lower TDF value in particular gives unrealistically high TP values for corals, we have here elected to use the same β and TDF values used for deep sea proteinaceous corals in McMahon et al. (2018).

2.8 Statistics and interpretational framework

We discuss coral data in the context of different regions of degradation, described by ranges of radial distance along the skeletal disc. The subfossil coral is discussed mainly in terms of three separate zones for bulk isotopic and C/N data: 1) outer diagenetic horizon (0-10 mm), as defined by very rapid changes in both C/N and isotope values, 2) inner, intermediate zone (10-36 mm) defined by only minor offsets from expected values, and 3) the innermost most protected zone (>36 mm), with C/N values within expected ranges for live-collected specimens. However, for the mol% and CSIA-AA data these changes are only observed in the outermost layer. We therefore discuss these results only for the two distinct zones: 1) the outer diagenetic horizon (0-5 mm) and 2) the inner layers from 10 mm to the skeleton's center. For data from a live-collected

coral there are no analogous degradation zones, however here we group results to separate preindustrial samples from the Industrial Revolution, using 1900 CE based on coral-specific age models as a comparison of data more comparable to the subfossil coral.

For CSIA-AA comparisons between live and subfossil specimens and within the subfossil coral (0-5 mm versus >10 mm), the AA isotope data were normalized by taking each individual AA isotope value and subtracting the average value of all total hydrolysable AAs (THAA) in that sample, to allow direct examination of biosynthetic patterns (after McCarthy et al., 2007) without the confounding variable of differential δ^{15} N baseline. To test for significant differences across zones, measured parameters were compared using two-sample group t-tests, assuming unequal variances with 95% confidence intervals. Statistics were calculated using Real Statistics Resource Pack software (Release 6.2; Zaiontz, 2019).

3. Results

The live-collected specimen had a radius of 17 mm and radiocarbon analyses (n = 11) indicated an age of \sim 710 years (research data 1). The subfossil specimen had a radius of 46 mm and radiocarbon analyses (n = 9) indicated an age of 1,890 yrs (\sim 9,670 to 11,560 years BP; Fig. S2, research data 2).

3.1 Scanning Electron Microscopy

Under 125x magnification, the live-collected coral skeleton exhibited concentric growth layers, exaggerated by the presence of desiccation cracks generated during sample drying, aligned parallel to the growth layers (Fig. 1A). Under 1250x magnification, the live-collected coral growth layers were imaged as <1 µm thick sheets of tightly woven fibers (Fig. 1B). For the subfossil coral, the outer skeleton appeared less dense (Fig. 1C) and exhibited a flakey microstructure with an absence of the tightly woven fibers (Fig. 1D). The inner section of the

same subfossil coral appeared less altered compared to the outer skeleton and retained a concentrically layered appearance (Fig. 1E) along with some of the woven fibrous character, despite the presence of flakey microstructure (Fig 1F).

3.2 C/N ratios

The C/N values from all subsamples of the live-collected modern coral averaged 2.75 \pm 0.11 and were invariant within the analytical error. C/N values were higher in the subfossil specimen, increasing from 3.12 ± 0.05 (n = 18) in the innermost skeleton, to 3.28 ± 0.12 (n = 88) in the middle 10-36 mm zone of the skeleton, to 3.36 ± 0.16 (n = 88) in the outer 10 mm of the skeleton. Acidification resulted in small decreases of 0.09-0.14 in C/N ratios compared to non-acidified samples for the intermediate and innermost layers, which was within instrumental error of the non-acidified sample C/N ratios, and more substantial decreases of 0.32–0.68 in C/N ratios compared to non-acidified samples in the outer 10 mm (n = 3, research data 3 and 4).

The mean elemental weight percent of subfossil samples for the outermost layer (0-10 mm) was 4.7 ± 0.9 wt% C and 15.7 ± 2.6 wt% N (n = 88), with a low value of 2.9 wt% C and 10.7 wt% N observed in the outermost 0.1 mm. The inner intermediate zone (10-36 mm, n = 88) mean elemental weight percent was 5.4 ± 0.8 wt% C and 17.6 ± 2.4 wt% N with no clear trend. The innermost zone (>36 mm, n = 18) mean was 7.0 ± 0.7 wt% C and 21.8 ± 2.1 wt% N (research data 4), falling within the range of modern specimens.

3.3 AA Molar Distribution

The modern coral AA mol% values (Fig. 3, research data 5) for all AAs recovered were consistent with previous results for AA composition of K. haumaeea gorgonin (Druffel et al. 1995; Goodfriend, 1997; Sherwood et al. 2014). However, for the subfossil coral the mol% value of Gly alone was much lower (29.0 \pm 3.8%) than observed in the modern coral (52.4 \pm 2.4%;

Fig. 3B). When Gly was removed from the relative mol% calculation then the mol% distribution of remaining AA was essentially identical between subfossil and modern corals (research data 7.3) with only the mol% values for Ser, Val, Pro, and Thr showing small, but significantly different values between the subfossil (>10 mm) and live-collected coral (p = <0.002, research data 7).

Within the subfossil coral zones there were no significant differences in relative mol% for Ala, Thr, Ser, Val, Leu, Ile, Pro, and Phe between the inner (>10 mm) and outer (0-5 mm) layers (research data 7). Five other AAs did have small but statistically significant changes in mol% from the inner (>10 mm) to outer (0-5 mm) layers (Fig. 3A): decreases in Tyr (-3.2%, p = 0.023), Lys (-3.9%, p = 0.001), and increases in Asp (+1.9%, p = 0.008), Gly (+3.7%, p = 0.02), and Glu (+0.9%, p = 0.06).

3.4 Bulk δ^{15} N and δ^{13} C Results

Bulk δ^{15} N values in the Cross Seamount live-collected coral were $11.2 \pm 0.5\%$ (n = 290) before the Industrial Revolution (1270-1900 C.E.) with a high of 12.5% in ~1410 C.E. During the 1900's Industrial Revolution the δ^{15} N values declined steadily to a low value of ~8.8% in the outermost layers (research data 3). Mean bulk δ^{13} C values in the live-collected coral skeleton from the preindustrial era (prior to 1900 C.E.) were -16.3 \pm 0.3% (n = 290), reaching a high of -15.5% during the 1620-1650s C.E. Similar to bulk δ^{15} N values, δ^{13} C values also declined after the 1900s to the lowest observed value of -17.2% in the outermost layers (research data 3).

Subfossil coral skeleton $\delta^{15}N$ values were overall more positive than the live-collected coral, ranging from 12 to 20% (research data 4). Within the subfossil coral the outermost $\delta^{15}N$ values (0-10 mm) increased by ~7% relative to the mean to a high of ~20.1% in the outer ~1 mm, while the intermediate region (10-36 mm) mean value was $13.7 \pm 0.5\%$ with no temporal

trend (n = 88; Fig. 2B). The innermost zone (>36 mm) mean δ^{15} N value was (12.6 ± 0.6%; n = 18) and was slightly lower relative to the intermediate zone (Fig. 2B).

The bulk δ^{13} C values in the subfossil coral ranged from -17.3 to -14.6‰ over the entire record (Fig. 2C), very similar to the modern coral from this site as well as to other coral records reported from the North Pacific Subtropical Gyre region (McMahon et al., 2015). Similar to the δ^{15} N data, there was a large (~2‰) and nearly monotonic increase in δ^{13} C values in the outer layers (0-10 mm) of the skeleton. The intermediate region (10-36 mm) mean value was -16.5 ± 0.4‰ (n = 88) and the innermost (>36 mm) mean value was -17.0 ± 0.3‰ (n = 18). Similar to C/N results discussed in Section 3.2, acidification prior to EA analysis reduced δ^{13} C values primarily in the outer 0-10 mm layers (0.6-1.4‰ lower relative to unacidified skeleton; n = 3) and to a lesser extent in intermediate region (10-36 mm; 0.4-0.9‰ lower relative to unacidified skeleton; n = 3). There were no significant differences in δ^{13} C values due to acidification observed in the innermost zone (>36 mm) (Fig. 2C, research data 4.2). While these results suggest progressive influence of authigenic calcite, under a microscope there were no visible formation of bubbles when raw coral material was subjected to 1 N HCl at room temperature.

3.5 CSIA-AA δ^{13} C data

The normalized $\delta^{13}C$ CSIA-AA values ($\delta^{13}C_{norm-AA}$) showed very similar biosynthetic patterns between the modern specimen and the inner subfossil coral layers (>10 mm, Fig. 4). Within the subfossil coral, $\delta^{13}C_{norm-AA}$ values also remained similar between the subfossil's inner (>10 mm) and outer (0-5 mm) regions (Fig. 4), in contrast to the large changes observed in $\delta^{15}N_{norm-AA}$ values in the outermost horizon (Fig. 5). Comparing the normalized patterns of the pre-industrial live-collected (n = 3) and subfossil (inner >10 mm, n = 6) corals only two non-essential AAs had statistically different $\delta^{13}C_{norm-AA}$ values (Asp -2.3‰, p = 0.01, Pro +1.4‰, p =

0.03). The mean essential AA $\delta^{13}C_{EAA}$ values (Phe, Thr, Ile, Leu, Val, Lys) of deep-sea corals have been shown to directly reflect $\delta^{13}C$ baseline of export production (Schiff et al., 2014, Shen et al. 2021). The live-collected Cross Seamount coral (excluding the rapidly shifting regions after the Industrial Revolution) had a mean essential $\delta^{13}C_{EAA}$ value of -18.6 \pm 0.3‰ (n = 3, research data 11). The subfossil Cross Seamount inner layers $\delta^{13}C_{EAA}$ values (-16.0 \pm 1.5‰; n = 6, research data 12) were +2.6‰ more positive than the modern specimen from the same location (Fig. 6). The subfossil coral's outer layers (0-5 mm) had a mean $\delta^{13}C_{EAA}$ value of -17.1 \pm 0.7‰ (n = 2, research data 12), and there were no significant differences in $\delta^{13}C_{EAA}$ values between the normalized outer (0-5 mm, n = 2) and inner (>10 mm, n = 6) subfossil coral zones (Fig. 4, research data 13).

3.6 CSIA-AA δ¹⁵N data

Normalized CSIA-AA $\delta^{15}N$ patterns ($\delta^{15}N_{norm-AA}$) were very similar between the subfossil coral inner (>10 mm) layers and modern coral (Fig. 5, research data 8 and 9), consistent with the similarity observed in AA molar composition (with the sole exception of Gly). Comparing $\delta^{15}N_{norm-AA}$ values between the subfossil inner layers (>10 mm, n = 6; Fig. 5; blue filled circles) and the pre-industrial live-collected (n = 3; Fig. 5; yellow filled circles) coral, all $\delta^{15}N_{norm-AA}$ values except for Glx and Ile fell within one standard deviation of modern coral data. Gly and Ile had clear offsets from modern coral $\delta^{15}N_{norm-AA}$ patterns (Glx +3.4‰, p = 4.6E-5 and Ile -7.2‰, p = 0.002). Four additional AAs also had smaller offsets between modern and subfossil (>10 mm) coral $\delta^{15}N_{norm-AA}$ values, which while statistically significant for these runs, were also not notably different from typical analytical variation for GC-IRMS analyses (Asx +1.7‰, p = 0.02, Ser +2.1‰, p = 0.02, Lys +2.5‰, p = 0.004, and Phe +1.5‰, p = 0.02;

research data 10). A sample $\delta^{15}N$ CSIA-AA chromatograph showing peak separation for both modern and subfossil coral hydrolysate is in the supplemental material (Fig. S1B). Mean THAA $\delta^{15}N_{norm-AA}$ values were 17.7 \pm 1.0% (n = 5) for the outer diagenetic horizon (0-5 mm), while the inner layers (>10 mm) mean THAA $\delta^{15}N_{norm-AA}$ values were 19.2 \pm 0.8% (n = 6). This offset in THAA $\delta^{15}N_{norm-AA}$ values was in the opposite direction of the bulk $\delta^{15}N$ trend (Fig. 6).

In contrast to the similar and very consistent CSIA-AA patterns observed in the inner >10 mm layers described above, the $\delta^{15}N_{norm-AA}$ values in the outer seawater exposed layers were highly variable, with some more positive (Asx, Lys, Gly, Ala, Val, Ser, Leu; Fig. S3), others more negative (Ile, Thr, Glx, Pro; Fig. S4), and some varying with no consistency across subsamples analyzed (Phe, Tyr; Fig. S5). After normalization to THAA (proxy for average protein $\delta^{15}N$ value) there were also significant differences in $\delta^{15}N_{norm-AA}$ patterns between the outer diagenetic horizon (0-5 mm, n = 5) and inner layers (>10 mm, n = 6) (Fig. 5; red vs. yellow filled circles). These normalized values, reflecting the relative biosynthetic offset from average protein, were substantially different for most AAs: Asx (+2.3‰, p = 0.01), Gly (+2.1‰, p = 0.006), Lys (+1.8‰, p = 0.02), Ala (+2.8‰, p = 0.03), Val (+3.0‰, p = 0.03), Pro (+2.4‰, p = 0.03), and Thr (-14.5‰, p = 0.01; Fig. 5, research data 10).

3.7 Trophic and Degradation Proxies

Consistent with the individual AA isotope differences presented in Section 3.5, there were very large differences in the ΣV parameter for microbial degradation and protein resynthesis between modern and subfossil corals, in particular between the inner verses outer zones of the subfossil specimen. Due to the uniquely large $\delta^{15}N$ offset of Ile (-7.2%) between live-collected and subfossil specimens, ΣV was calculated both with and without Ile. The modern specimen had very consistent standard ΣV values, mean 2.7 ± 0.1 (3.0 \pm 0.2 when Ile

was excluded, n = 4, Fig. 6C). The subfossil inner (>10 mm) layers, where most $\delta^{15}N_{AA}$ data were consistent with live-collected coral, also had a consistent but elevated standard ΣV value of 4.0 ± 0.3 using all AA (n=6). However, this result was very strongly driven by Ile $\delta^{15}N$ values alone. Recalculating ΣV without Ile, the inner subfossil coral average ΣV was 3.4 ± 0.2 (n = 6), comparable to data for the modern coral. Finally, the diagenetic horizon (0-5 mm) subfossil coral layers had very high ΣV values, reaching among the highest values (range 5-6, Fig. 6C, research data 9).

TP_{CSIA-AA} Skeleton values also varied substantially within the subfossil coral but were again similar between the inner subfossil layers (>10 mm) and the modern coral. Subfossil inner layers (>10 mm) had TP_{CSIA-AA} Skeleton values with a mean of 3.1 ± 0.1 (n = 5), very close to modern coral values (3.3 ± 0.5 , n = 4), while the subfossil outer layers reached a low TP_{CSIA-AA} Skeleton of 1.2 (at 2.8 mm) in the same region with highest Σ V (Fig. 6D). Alternative calculations for trophic position were also examined, all indicating similar trends within and among zones (Fig. S6).

4. Discussion

Understanding the long-term preservation of deep-sea proteinaceous coral skeletons is critical to extending the time horizon of paleo-applications using these valuable bioarchives. Comparisons of subfossil (~9.6-11.6 kyr BP) and modern *K. haumeaae* skeletons across a wide range of physical features, bulk chemical composition based on C/N, bulk δ^{13} C and δ^{15} N values, molecular level AA molar percentages and isotope compositions, and CSIA-AA parameters for degradation (Σ V) and trophic position (TP_{CSIA}) show excellent preservation of physical and geochemical composition in the inner subfossil coral skeleton. These findings lend confidence to the paleo-application of geochemical proxies in deep-sea proteinaceous coral skeletons to

reconstruct biogeochemical cycling, plankton community trophic dynamics, and export production back through the Holocene. At the same time, we also clearly identified a very distinct seawater exposed, outer diagenetic horizon of the skeleton with both abiotic alteration (e.g., loss of glycine, potential carbonate addition) and biotic degradation (e.g., increased variability in AA isotope values, ΣV, TP_{CSIA-AA Skeleton}) accompanied by physical changes in the skeleton matrix (SEM images). Identification of this region will help to avoid potential misinterpretation of geochemical data in degraded regions of these archives.

4.1 Physical structure: matrix changes in subfossil coral

Skeletons of *K. haumeaae* exhibit concentric growth layers composed of a tightly bound fibrillar protein, similar to other proteinaceous corals (Goldberg, 1976; Noé and Dullo 2006; Sherwood et al. 2006). Visually there was little difference in skeletons between the live-collected and subfossil specimens without magnification. While the subfossil disk was lighter in color, with a drier, flaky outer crust, there was no visual indication of the physical or chemical degradation zonation. Specifically, the diagenetic horizon (outer 10 mm) discussed extensively in subsequent subsections, could not be visually identified.

Under higher magnification (SEM) structural differences between the live-collected and subfossil specimens were readily apparent (Fig. 1). For the live-collected specimen the regular banded fibrous layers were clearly visible in SEM images (Fig. 1A, 1B). This suggests while the modern skeleton itself is not living, it was physically very well protected from the influence of ocean water by the living outer polyp colony and intact outer skeleton. It has been hypothesized that the tightly woven fibrous structure of proteinaceous coral skeletons contributes to degradation resistance by preventing seawater penetration (Druffel et al., 1995), with the implication being that physical protection slows down biological as well as abiotic compositional

changes. Similar physical protection of organic matter is well known in a range of matrixes including as eggshell/bone (e.g., Hendy, 2021) and soil organic matter (e.g., Krull et al., 2003). In shallow water carbonate corals it is only after the polyps die that the skeleton is exposed and significant colonization by bacteria, borers, and physical grazing occurs (Le Campion-Alsumard et al. 1995). The protection of the inner coral skeleton is therefore likely applicable to other genera of corals as well as skeletons of different ages but further research is necessary to confirm this.

The subfossil coral skeleton showed hallmarks of matrix degradation at both a macro and microscale level, particularly in the outer most, seawater exposed zone of the skeleton (Fig.1). Visually, a more brittle and paper-like apparent character in SEM images of the very outermost layers (<0.1 mm) suggest possible structural changes in the protein matrix. Furthermore, SEM imaging showed clear loss of tightly woven fibers and a flakey microstructure (Fig 1C, 1D). Overall, the loss of microfiber banding and less dense sheeting in the subfossil coral suggests intensive structural degradation in the outermost, most seawater impacted region (Fig. 1C, 1D), likely due to a combination of degradation with time and seawater exposure/infiltration. We hypothesize that these physical changes could provide more surface area for microbial activity in outer layers (Ingalls et al. 2003), in contrast to the denser, better protected inner layers. Finally, we note that the physical transition from the outer layers' distinctive plate-like structure to more dense layers in the inner layers appears gradual, and we could not clearly identify the distinct chemical diagenetic horizon in SEM images which appeared quite sharp in the geochemical proxies.

4.2 Elemental Composition Changes

The C/N ratio of unaltered gorgonin can be used as a reference to evaluate changes in skeletal composition associated with degradation, since it should be both fixed and predictable within any coral species. A similar C/N ratio approach has commonly been taken to assess both diagenesis and exogenous organic contamination impacting the integrity of collagen, which has structural similarities to gorgonin (e.g., Ambrose and Norr, 1992).

The C/N ratio of proteinaceous skeleton material from live-collected K. haumeaae in this study (2.8 \pm 0.1) agrees with a number of previous studies on live-collected K. haumeaae from the Hawaii Islands (2.7-3.0 Sherwood et al., 2014, McMahon et al., 2015) and the Atlantic (2.8-3.0 Druffel et al., 1995, Goodfriend 1997). It should be noted that most previous studies used acidification prior to EA analysis to ensure no influence of inorganic carbonates on C/N ratios. Prior published data using acidified samples (e.g., Guilderson et al., 2013, Glynn et al., 2019) has shown indistinguishable C/N values from those we observed in our live-collected non-acidified specimens, all suggesting that a C/N ratio of 2.7-3.0 would be expected for intact / non-degraded K. haumeaae skeletons, which is similar to the expected C/N of pure protein (\sim 3), and that acidification does not change greatly these values for the intact organic matrix after any carbonate is removed.

However, in our non-acidified subfossil skeleton samples, we observed elevated C/N values (+0.1-0.8 C/N units higher versus the live-collected *K. haumeaae* skeleton; *results 3.2*; Fig. 2). These findings corroborate a recent study showing that *non*-acidified subfossil coral C/N values can deviate well above 3.0, particularly in outer exposed layers (Glynn et al. 2019). These deviations suggest either carbonate precipitation or selective organic N loss with degradation in exposed specimens. We also observed an essentially linear shift in C/N ratios in the subfossil

coral outer diagenetic horizon (0-10 mm), culminating in the highest C/N ratios at the seawater interface (C/N = 3.7, Fig. 2A). Further, while acidification did reduce C/N ratios across the entire coral transect, acidification did not "restore" C/N values in the outer diagenetic horizon to the reference value. This strongly suggests that both carbonate formation and organic degradation are simultaneously occurring. Finally, the fact that the inner skeleton layers of the subfossil coral had C/N ratios within instrumental error to fresh gorgonin, regardless of acidification (average offset +0.1 C/N units in >10 mm layers, research data 4), strongly indicates that inner skeleton layers remain well protected from degradation even in a ~10 kyr specimen. Overall, we propose C/N ratios *after* acidification can be used a simple metric to assess degradation state in non-living coral sea floor specimens: C/N ratios >3 indicate appreciable degradation of the gorgonin organic matrix, suggesting great caution in interpreting bulk δ^{13} C and δ^{15} N values (as discussed in Sections 4.3-4.4). We recommend that future subfossil coral studies analyze C/N to test degradation state prior to interpretation of environmental signatures.

4.3 Mechanisms of elemental C/N and bulk δ^{13} C changes

4.3.1. Glycine loss

The acidification tests described in Section 4.2 suggest that elevated C/N values are at least in part due to the presence of secondary authigenic carbonate. However, a change in organic gorgonin molecular composition is an additional possibility. While molecular AA data indicate a relatively similar composition for most AAs between subfossil and live-collected coral skeleton (Fig. 3B, results 3.3), glycine (Gly) was the major exception. The ~50% lower Gly contribution in all layers of the subfossil specimen compared with modern gorgonin suggests a major organic structural change. At the same time, Gly also has the lowest C/N value of any AA (2.0). Therefore, the large loss of glycine must contribute at least in part to higher C/N values

observed throughout the subfossil skeleton. A mass balance calculation based on the modern coral mol% values can broadly constrain this effect: our observed change in Gly from 52% in live-collected skeleton to 23% in subfossil skeleton would be expected to increase C/N by 0.35-0.41, assuming that all other organic composition remains constant. We note that while acidification results show this cannot be the only process at work, at the same time this result is quite similar to the actual C/N offsets observed between the subfossil inner layers (>10 mm) and the average of modern corals (research data 3). One caveat to this estimate is that our acid hydrolysis-based analytical method cannot measure Histidine. Histidine is an N-rich (low C/N) AA that is very abundant in many gorgonin-based proteins (18-30%; Druffel et al., 1995, Goodfriend, 1997) such that any major "hidden" changes in this AA could have substantial C/N impacts. However, the fact that our simple calculation based on Gly loss alone is consistent with both observed C/N and molar data suggests that loss of glycine is likely the dominant organic process driving the C/N offset between modern and subfossil corals over millennial timescales.

The mechanism leading to large glycine losses from coral skeleton over millennia is uncertain. However, the fact Gly appears to be lost and not gained in subfossil corals compared with modern corals, coupled with only minor changes in other AA molar composition (results 3.3), strongly suggests an abiotic mechanism. Gly mol% increases are a widely used AA indicator for microbial degradation (e.g., Dauwe et al., 1999; Yamashita and Tanoue, 2003; Kaiser and Benner, 2009), making a nearly 50% Gly reduction inconsistent with typical biologically-mediated changes. Further the widely used Degradation Index (DI; based on AA mol% shifts observed with marine organic matter degradation; Dauwe et al., 1999) yields DI values close to "fresh" plankton in the inner coral (Fig. S8). In fact, most of the subfossil coral DI values *elevated* (indicating *less* degradation) versus the values of the modern coral specimen.

As discussed further below (section 4.5) this is likely due in part to the unique AA composition of the gorgonin skeleton, rather than microbial degradation of subfossil coral skeleton.

We hypothesize that abiotic glycine decarboxylation may be the main mechanism for subfossil coral Gly loss. The spontaneous aqueous decarboxylation of free glycine is well known, whereby water molecules assist with proton transfer cleaving the Gly C-N bond, resulting in degradation of Gly (e.g., Catão and López-Castillo, 2018 and references within). As structurally the simplest of all AAs, glycine (C₂H₅NO₂) is thermodynamically favored to remove the amide group to form bicarbonate and also requires the least water (4H₂O) to do so (LaRowe and Van Cappellen, 2011). We note that this process may also contribute to authigenic carbonate formation, potentially accounting for some of the C/N offset between the acidified and non-acidified data. While this reaction has not been previously reported for glycine bound in a proteinaceous structure, it would provide a potential mechanism for Gly degradation in the seawater exposed outer diagenetic horizon of coral skeletons over ~10 kyrs.

Gly loss would also be consistent with physical structure changes, as Gly plays an important role in holding adjacent layers together in *K. haumeaae* skeletons (Druffel et al. 1995). We therefore further hypothesize that selective abiotic Gly loss contributes to the altered physical matrix observed in subfossil coral SEM images (Fig. 1A, B). Finally, we note that while the dramatic Gly molar depletion (~50%) is clear in all subfossil coral samples, the more minor Gly changes observed from inner vs. outer subfossil skeleton (~5 mol%; Fig. 3) are in the opposite direction. While these more minor offsets are approaching the analytical variation of chromatography methods, this result at least suggests that some addition biotic degradation of the protein matrix is occurring, superimposed on the earlier rapid and far larger abiotic decarboxylation. Investigation into whether AA degradation in protein-bound AAs follows the

same hydrolysis-based degradation pathways as free AAs is necessary to validate this hypothesis. Such work would shed additional light on other unknown compounds besides the dominant proteinaceous material in these types of deep-sea corals that may also be altered during this degradation process.

4.3.2 Secondary authigenic carbonate

Higher C/N ratios and δ^{13} C values observed after acidification must in part be due to carbonate precipitation, particularly in the outermost coral layers (0-10 mm) most subjected to seawater infiltration. Though of note, even if the inner layers (>10 mm) are protected from direct seawater influence, if our hypothesis regarding Gly decarboxylation is correct then inorganic carbonate could also accumulate here (Catão and López-Castillo, 2018). While seawater carbonate precipitation is therefore never mutually exclusive from an abiotic decarboxylation mechanism, one major difference is that carbonate precipitation should lead to a contemporaneous increase in bulk δ^{13} C values. Glycine loss is more difficult to constrain, however it would most likely work in the opposite direction (i.e., *decreasing* bulk δ^{13} C values), because Gly is typically ~3% higher in δ^{13} C value compared to the average of all proteinaceous AAs (Shen et al. 2021, McCarthy et al., 2013).

As carbonate δ^{13} C endmembers can be estimated, the potential quantitative influence of authigenic carbonate on bulk δ^{13} C values can be constrained using isotope mass balance. If we assume a δ^{13} C value of 1‰ for dissolved inorganic carbon (DIC) and a fractionation (ϵ) from DIC to calcite of 1‰, then authigenic calcite should have a δ^{13} C value of ~2‰ (Romanek et al., 1992; Quay et al., 2003). This means that the maximum observed offset of ~1.4‰ between the acidified and non-acidified samples in the outermost 1 mm (Fig. 2C) would require ~7-8% of

total C to be present as calcite precipitate. Returning to our C/N data, if the "fresh" gorgonin C/N is \sim 2.8, then 8% carbonate accumulation (as a fraction of total C) would cause C/N to increase to \sim 3.0. This shift of \sim 0.2 C/N would therefore represent approximately half of the \sim 0.4 C/N shift we calculated above from loss of glycine.

Currently no studies have focused on carbonate precipitation in deep-sea proteinaceous coral skeletons. Estimates of sedimentary secondary authigenic carbonate formation can reach as high as 10% in high depositional regions (Sun and Turchyn, 2014). While the mechanism for sedimentary authigenic carbonate formation is clearly different than in deep-sea corals, and in particular is likely much more dependent on pH and degrading organic matter, nevertheless we note that the similar magnitudes of maximum carbonate in our outer coral layers and in sediments at least suggest that this mass balance estimate of possible secondary authigenic carbonate formation is not unreasonable. Some additional carbonate precipitation could also be related to respiration of the skeletal organic matter should seawater intrusion supply enough oxygen that pH does not facilitate dissolution. Particularly in the outer diagenetic horizon, both processes are likely contributing to observed isotope shifts. For sediments, locations with enhanced microbial respiration tend to have the largest amount of authigenic carbonate formation, because microbes affect pore water chemistry by converting organic matter to CO₂, which then precipitates as carbonate (e.g., Sun and Turchyn, 2014). Further analysis to discover whether unique microbial populations facilitate deep-sea coral degradation and how the deposition and degradation of sediments upon dead skeletons impact water chemistry should be conducted.

4.4 Biological degradation in seawater exposed gorgonin: impact on bulk $\delta^{15}N$ values and

CSIA-AA parameters

576

577

578

579

580

581

582

583

584

585

586

587

588

589

590

591

592

593

594

595

596

597

598

In contrast to the protected inner layers, the outer diagenetic horizon (0-10 mm) layers show clear evidence of microbial degradation, discernible at the molecular level. While carbonate precipitation and abiotic Gly loss described in Section 4.3.1 can account for some of the C/N and isotope ratios changes (Fig. 2), the $\delta^{15}N_{AA}$ values in the outer layers bear the signature of microbial resynthesis with highly elevated ΣV values in comparison to both the modern coral specimen and the subfossil coral interior (McCarthy et al., 2007; Fig. 6C). The ΣV parameter quantifies variability in $\delta^{15}N_{AA}$ patterns as a measure of progressive degradation and reflects the selective microbial resynthesis of individual AAs (McCarthy et al., 2007, Batista et al., 2014, Sauthoff et al., 2016, Ohkouchi et al, 2017). Together with strongly elevated bulk $\delta^{15}N$ values, ecologically unrealistic CSIA-AA trophic position values (Fig. 6D; discussed in Section 4.4.1), and dramatic outer layer structural changes seen in SEM imaging (Fig. 1), this data suggest significant biological degradation of the outer gorgonin matrix after direct contact with seawater.

We propose that the coupled large changes in bulk $\delta^{15}N$ and $\delta^{13}C$ values observed in the diagenetic horizon likely reflect combined abiotic and biological effects of oxic seawater exposure. Multiple lines of evidence support this conclusion. First, the large and almost linear increase in $\delta^{15}N$ values of ~7‰ in the outer layers is consistent with expected impact of microbial degradation on organic matter, typically imparting a strong increase in the $\delta^{15}N$ values of the residual or substrate organic matter, with changes in $\delta^{15}N$ values up to 6‰ observed in sediments and suspended particles (Saino and Hattori, 1980; Saino and Hattori, 1987; Altabet, 1988; Lehmann et al., 2002). While some baseline $\delta^{15}N$ shift cannot be ruled out, the unidirectional change in $\delta^{15}N$ values in the outer coral is substantially greater than any documented change in comparable corals since at least the last 5 kyrs (Williams and Grottoli,

2010, Sherwood et al., 2014, Glynn et al. 2019). This suggests $\delta^{15}N$ baseline changes are exceedingly unlikely to be the main driver of the $\delta^{15}N$ change in the outer diagenetic horizon. Second, some part of the $\delta^{13}C$ value increases may also be due to microbial degradation removing the lighter ^{12}C from the skeleton, in addition to respiration contributing to carbonate formation discussed in Section 4.3.2. Given that our isotope mass balance exercise above suggests $\sim 1\%$ of the observed $\delta^{13}C$ change could be due to carbonate formation, this would theoretically leave another $\sim 1\%$ of the total shift observed in the outer layers due to a mechanism like microbial degradation.

Finally, we also evaluated the degradation index (DI) because is one of the most widely used degradation proxies in organic geochemistry, commonly applied in sediments, ocean particles, and other detrital organics (Dauwe et al., 1999). The underlying assumption of the DI index is that AAs have different and predictable relative lability to bacterial degradation of proteinaceous materials. However, the standard DI formulation does not appear to indicate lability in gorgonin as DI indicated more "degraded" values in the most protected inner coral layers, becoming "fresher" with progressive structural deterioration and alteration of other degradation metrics (Fig. S8). In particular in the outer diagenetic horizon where evidence of degradation seems unambiguous, DI does not change in a uniform manner. We hypothesize that either the very different AA composition of gorgonin (a very specific, single structural protein), or different mechanisms by which bacteria are able to degrade this material, underlie these observations. We conclude that standard DI is not a useful metric to evaluate relative degradation state/integrity of gorgonin structural protein but by utilizing skeletons spanning a variety of ages it should be possible to create a coral specific DI.

4.4.1 Preservation and likely fidelity of CSIA-AA parameters

Degradation in the outer diagenetic horizon had major impacts on two important CSIA-AA proxies of environmental biogeochemistry and trophic dynamics. TP_{CSIA-AA} is commonly applied in deep sea corals and sediments to indicate relative changes in planktonic food web structure (Batista et al. 2014, Sherwood et al. 2014, Sauthoff et al., 2016). It appears that microbial degradation in the outer subfossil coral material also strongly impacts TP_{CSIA-AA} skeleton, consistent with elevated ΣV data in this zone. Specifically, the lowest TP_{CSIA-AA} Skeleton value of 1.7 in the outer subfossil coral layers is more than a full trophic step lower than the inner (>10 mm) layers (TP_{CSIA-AA} Skeleton = 3.1 ± 0.1), with swings of ~1.5 trophic levels between adjacent samples (Fig. 6D). It seems very unlikely that large and rapid shifts in overlying plankton ecology and unrealistically low TP values occur only at the end of this coral colony's millennial lifespan. We note that the mean trophic-source $\delta^{15}N_{AA}$ offsets, often used as proxy for relative TP change that avoids issues of TDF and β selection, (McCarthy et al. 2007, Sherwood et al. 2011, Batista et al. 2014), show similar patterns. Together, these data indicate that TP_{CSIA} values are viable in the intermediate (transition) and inner most protected coral regions, but should not be trusted in the outer diagenetic horizon without corroborating evidence of minimal degradation (i.e., ΣV value and/or C/N ratio).

645

646

647

648

649

650

651

652

653

654

655

656

657

658

659

660

661

662

663

664

665

666

667

The significantly higher ΣV values in the outer zone of the subfossil coral skeleton (maximum 5.8, Fig. 6C) were clearly distinct from both the inner zone and modern corals and were consistent with strong microbial resynthesis. The ΣV values (3-4) observed throughout the inner subfossil coral are high relative to the range typically found in plankton or non-degraded proteinaceous materials (<2.0; McCarthy et al, 2007), and slightly elevated compared to modern coral specimens (~3.0; Sherwood et al., 2014; this study, Fig. 6). In the modern coral, the difference in ΣV value from fresh material has been attributed to the unique AA composition of

the gorgonin structural protein (Sherwood et al., 2014). However, note that the ~1 ΣV value offset between modern and inner subfossil coral layers is almost exclusively driven by changes in isoleucine. Without isoleucine, both modern and subfossil ΣV values are very similar (0.4 ΣV offset), which is consistent with the very similar CSIA-AA biosynthetic patterns (Fig. 5, 6B). This apparently singular $\delta^{15}N$ shift in isoleucine in the subfossil coral is puzzling. A unique isoleucine shift of this kind has never been observed in CSIA-AA $\delta^{15}N$ patterns for degrading OM; in fact here it might not be biological at all, given that it is observed even in the innermost, protected coral layers. Further research into this loss could shed more light on the mechanisms underlying multi-millennial gorgonin alteration. Overall, with the exception of Ile, bulk δ^{15} N values and $\delta^{15}N_{AA}$ patterns for all other AAs indicates that CSIA-AA proxies were well preserved in the inner coral layers. With the exception of threonine (Thr), a metabolic AA, and isoleucine (Ile) the scatter of the individual non-normalized as well as THAA-normalized values in the ≥10mm interior of the sub-fossil specimen were similar to the scatter in not only the modern Cross Seamount specimen, but a larger data-set in near-modern specimens from off Oahu (Sherwood et al., 2014). Thus, and in general, the inner layers are preserved with similar isotopic values Some variability does occur in individual AA data points as expected for degraded or complex matrixes, however isolated individual AA data points may be impacted by analytical variability thus we use averages of the different regions and propagated error to show the inner layers are typically preserved with similar isotopic values (Fig. S3-S6).

687

688

689

690

668

669

670

671

672

673

674

675

676

677

678

679

680

681

682

683

684

685

686

4.5 Inner coral preservation of CSIA-AA parameter integrity

The excellent preservation of expected molecular geochemistry parameters (e.g., mol%, ΣV , TP_{CSIA}) in the inner coral (>10 mm) strongly suggests that beyond the outer diagenetic

horizon, subfossil deep-sea proteinaceous skeletons remain viable as <u>paleoenvironmental</u> bioarchives. As baseline δ^{13} C or δ^{15} N values of primary production from ~9.6-11.6 kyr BP cannot be known, it is not possible to directly confirm this hypothesis. However, there are ways to evaluate the integrity of CSIA-AA values by examining CSIA-AA patterns and source AA values in order to reconstruct paleo-export production values.

691

692

693

694

695

696

697

698

699

700

701

702

703

704

705

706

707

708

709

710

711

712

713

The first way is specifically evaluating relative CSIA-AA patterns with those from marine primary production and sinking particles (Fig. S9). The observation of expected patterns in normalized CSIA-AA data provides strong evidence for the preservation of individual AA isotope values since degradation processes scrambles CSIA-AA patterns and degradation is unlikely to alter values of every AA in exactly the same way (e.g. McCarthy et al., 2007, Okhouchi et al., 2017). The essentially identical $\delta^{15}N_{norm-AA}$ patterns observed for almost all AAs (Fig. 5; Results 3.5) in the inner (>10 mm) zone of the subfossil coral match those CSIA-AA biosynthetic patterns expected for live-collected deep sea corals, which consume photosynthetic marine algae and sinking particles (Fig. S9; Shen et al., 2021, McCarthy et al., 2013, this study). Average source and trophic AA group values can represent an additional check on the influence of any possibly anomalous individual AA isotope changes with degradation (McCarthy et al., 2007). Both these metrics also show stable plateaus for the inner (>10 mm) layers of the subfossil coral (Fig. 6), consistent with the relatively low and stable ΣV values described earlier, and again supporting good preservation of CSIA-AA δ^{15} N values in the protected interior coral skeleton.

A second way to evaluate if AA values have been well preserved is to ask if shifts in predicted 'baseline" correspond with records from other archives in this region. The shift in "baseline" $\delta^{15}N$ values indicated by CSIA-AA (e.g., Source AA's Lys, Phe, Tyr; non-

normalized) are in fact consistent with expected changes in this Pacific region. The shift in average source AA values indicates a change in the source nitrate $\delta^{15}N$ value of ~3% between the subfossil inner layers (10-11.6 kyrs BP; $\delta^{15}N_{\text{source}} = 9.4 \pm 0.5\%$) and the modern coral $(\delta^{15}N_{source} = 6.3 \pm 1.3\%)$, research data 8 and 9). Based on the molecular changes found in this study, such as the shift in Gly from 52-26%, these composition changes may account for a ~1\% increase in bulk $\delta^{15}N$ over this timeframe. This would account for a third of the ~3\% change between modern and inner subfossil, leaving ~2\% attributed to environmental change, which is still within range suggested by sedimentary margin records (~1-5‰; Tesdal et al. 2013). The CSIA-AA δ^{13} C (mol\% weighted THAA; a proxy for baseline) also supports a baseline shift between the modern coral (-9.9 \pm 0.7%; n = 3) and the subfossil coral (-11.9 \pm 0.2%; n = 6), again consistent with the export production δ^{13} C values that have increased by ~2\% from the Younger Dryas (~12 kyrs ago) to the late Holocene in Pacific Margin sedimentary δ^{13} C records (references within Tesdal et al. 2013). Together these results also suggest that $\delta^{13}C_{AA}$ plankton community fingerprinting approaches recently demonstrated in ~1000 yr old gold corals (McMahon et al., 2015) may also be able to reconstruct plankton community structure of exported production from subfossil corals, assuming that proper phytoplankton end-members are used for a given time period.

5. Summary and Conclusions

714

715

716

717

718

719

720

721

722

723

724

725

726

727

728

729

730

731

732

733

734

735

736

By comparing a subfossil (~9.6-11.6 kyr BP) *K. haumeaae* coral skeleton with a live-collected specimen from the same seamount in Hawaii, this study documented microstructural, molecular, and geochemical changes accompanying degradation of the proteinaceous coral gorgonin matrix. These changes occurred primarily in the outermost skeleton, which we hypothesize are due to a combination of abiotic and biotic degradation as a function of contact

with oxic seawater for \sim 10 kyr. The physical structure of the outer subfossil coral showed pronounced loss of banding, shifting to a randomized plate-like and presumably less dense structure. We hypothesize that these structural changes contributed to seawater penetration and subsequent microbial activity that altered skeleton molecular and geochemical values in this outer diagenetic horizon. At the molecular level, all layers of the subfossil coral had only about half the expected molar glycine content of live-collected coral skeleton, while the effects of acidification on skeleton δ^{13} C values indicated significant authigenic carbonate formation, particularly in the outer zone. We hypothesize that this carbonate formation was enhanced by the abiotic degradation of glycine and associated production of bicarbonate. However, despite all these changes, molar compositions for all other AAs were similar to the live-collected counterpart for all but the outermost (0-10 mm) layers.

The outermost ~10 mm of the subfossil coral was distinct in every molecular parameter, with extensive changes consistent with both microbial degradation and substantial carbonate precipitation, both likely linked to seawater exposure. Large linear increases in bulk δ^{13} C and δ^{15} N values, coupled with high values of the degradation parameter Σ V and anomalous CSIA-AA trophic position values indicated extensive, progressive, and easily identifiable microbial degradation. Together, these shifts are consistent with progressive organic degradation with seawater infiltration and attendant gorgonin physical structure breakdown, occurring in this coral at approximately 1 mm per 1000 yrs.

In contrast to the outer diagenetic horizon, all the same proxies within the intermediate and innermost coral layers indicated excellent preservation of the gorgonin protein, in particular molecular level AA isotope values. We propose C/N ratio as a basic metric to evaluate skeleton integrity, where C/N values above 3 for this species indicate degradation extensive enough to

confound bulk isotope data interpretations. This should be supplemented by acid tests (or direct $%CaCO_3$ determination) to evaluate carbonate contamination. Further, we suggest that while the DI index appears to not function reliably in the gorgonin matrix, the CSIA-AA based ΣV metric beyond the typical gorgonin baseline value of 3.0 can provide clear information about microbial influence.

While gorgonin bulk isotope and elemental values can be strongly altered in the outer zone of subfossil specimens, CSIA-AA values and associated proxies appear to be far more robust to these degradation processes. In particular CSIA-AA proxies for isotopic baseline (Phe, mean source AA δ^{15} N values, and mean essential AA δ^{13} C values) appeared to be well preserved beyond the outer diagenetic horizon, with biosynthetic patterns very similar to both primary production and modern coral gorgonin for both δ^{13} C and δ^{15} N values. Even Gly, despite its very large molar loss, had normalized CSIA-AA patterns that matched those expected from modern corals for both δ^{13} C and δ^{15} N. The δ^{15} N values of Ile were one notable exception, with substantially elevated δ^{15} N values in all zones of the subfossil coral. To our knowledge, such shifts in Ile δ^{15} N values have not been previously observed, and based on these observations, we suggest that Σ V in protein corals should in the future be calculated without Ile.

Overall, the excellent CSIA-AA pattern preservation in the inner deep-sea proteinaceous coral skeletons on multi-millennial time scales indicates that source and essential AAs can be used to determine environmental information about export production and degradative processes in subfossil coral skeletons when C/N and ΣV values fall within expected ranges. We propose that a combination of elemental and CSIA-AA metrics can be used to readily gauge gorgonin integrity and screen subfossil samples for more reliable geochemical interpretations. This work opens wide potential to the use of CSIA-AA proxies for reconstructing baseline biogeochemical

cycling, export production dynamics, and algal trophic structure and community composition, at least back through the Holocene using the wealth of available subfossil specimens.

Acknowledgements

None of this work would have been possible without the captain and crew of the RV Ka'imikai-o-Kanaloa and the pilots and engineers of the Hawai'i Undersea Research Lab. Sample collection was funded by NOAA/NURP and the National Geographic Society (7717-04). A portion of this work was performed under the auspices of the U.S. Department of Energy (DE-AC52-07NA27344). The majority of the work presented here was funded by the National Science Foundation (OCE 1061689 and OCE 1635527 to TPG&MDM). D.S. Glynn was supported by a Eugene Cota-Robles Fellowship and a National Science Foundation Graduate Research Fellowship (NSF-GRFP; 1339067). We acknowledge Dr. T. Yuzvinsky for assistance

with sample preparation and electron microscopy and the W.M. Keck Center for Nanoscale Optofluidics for use of the FEI Quanta 3D Dualbeam microscope. Further thanks go to D. Andreasen, C. Carney, R. Franks and a team of undergrad interns (S. Kaplan, A. Jalali-Sohi, K. Miles, L. Gomez, Z. Wright) for laboratory assistance. Thanks to the assisting editors and anonymous reviewers for their feedback.

811

812

813

814

817

818

820

821

822

824

825

826

827

806

807

808

809

810

References

Altabet M. A. (1988) Variations in nitrogen isotopic composition between sinking and suspended particles: implications for nitrogen cycling and particle transformation in the open ocean. 815 Deep Sea Research Part A. Oceanographic Research Papers 35, 535–554. 816 Ambrose S.H. and Norr L. (1993) Experimental Evidence for the Relationship of the Carbon Isotope Ratios of Whole Diet and Dietary Protein to Those of Bone Collagen and Carbonate. In *Prehistoric Human Bone* (eds. J. B. Lambert, G. Grupe). Springer. pp. 1– 819 38. Batista F. C., Ravelo C. A., Crusius J., Casso M. A., and McCarthy M. D. (2014) Compound specific amino acid $\delta^{15}N$ in marine sediments: A new approach for studies of the marine nitrogen cycle. Geochimica et Cosmochimica Acta 142, 553–569. 823 Boyer T. P., Garcia H. E., Locarnini R. A.; Zweng M. M., Mishonov A. V., Reagan J. R., Weathers K. A., BaranovaO. K., Seidov D., Smolyar I. V. (2018) World Ocean Atlas 2018. Temperature and Dissolved Oxygen averaged over years 1955-2010 at 400m. NOAA Information, National Centers for Environmental

https://accession.nodc.noaa.gov/NCEI-WOA18 (accessed July-4-2021).

| 828 | Chikaraishi Y., Ogawa N.O., Kashiyama Y., Takano Y., Suga H., Tomitani A., Miyashita H., |
|-----|---|
| 829 | Kitazato H., and Ohkouchi N. (2009) Determination of aquatic food-web structure based |
| 830 | on compound-specific nitrogen isotopic composition of amino acids. Limnology and |
| 831 | Oceanography: Methods 7, 740–750. |
| 832 | Dauwe B., Middelburg J. J., Herman P. M. J., and Heip C.H.R. (1999) Linking diagenetic |
| 833 | alteration of amino acids and bulk organic matter reactivity. Limnology and |
| 834 | Oceanography 44, 1809–1814. |
| 835 | Druffel E. R. M., Griffin S., Witter A., Nelson E., Southon J., Kashgarian M., and Vogel J. |
| 836 | (1995) Gerardia: Bristlecone pine of the deep-sea? Geochimica et Cosmochimica Acta |
| 837 | 59 , 5031–5036. |
| 838 | Edinger E. N. and Sherwood O. A. (2012). Applied taphonomy of gorgonian and antipatharian |
| 839 | corals in Atlantic Canada: experimental decay rates, field observations, and implications |
| 840 | for assessing fisheries damage to deep-sea coral habitats. Neues Jahrbuch fur Geologie |
| 841 | und Palaontologie-Abhandlungen, 265 , 199. |
| 842 | Ehrlich H. (2010) Chitin and collagen as universal and alternative templates in biomineralization. |
| 843 | International Geology Review 52 , 661-699. |
| 844 | Glynn D. S., McMahon K. W., Guilderson T. P., and McCarthy M. D. (2019) Major shifts in |
| 845 | nutrient and phytoplankton dynamics in the North Pacific Subtropical Gyre over the last |
| 846 | 5000 years revealed by high-resolution proteinaceous deep-sea coral $\delta^{15}N$ and $\delta^{13}C$ |
| 847 | records. Earth and Planetary Science Letters 515, 145–153. |
| 848 | Goldberg W. M. (1974) Evidence of a sclerotized collagen from the skeleton of a gorgonian |
| 849 | coral. Comparative Biochemistry and Physiology Part B: Comparative Biochemistry 49, |
| 850 | 525–526. |

- 851 Goldberg W. M. (1976) Comparative study of the chemistry and structure of gorgonian and
- antipatharian coral skeletons. *Marine Biology* **35**, 253–267.
- 853 Goodfriend G. A. (1997) Aspartic acid racemization and amino acid composition of the organic
- endoskeleton of the deep-water colonial anemone Gerardia: Determination of longevity
- from kinetic experiments. *Geochimica et Cosmochimica Acta* **61**, 1931–1939.
- Guilderson T. P., McCarthy M. D., Dunbar R. B., Englebrecht A., and Roark, E.B. (2013) Late
- Holocene variations in Pacific surface circulation and biogeochemistry inferred from
- proteinaceous deep-sea corals. *Biogeosciences* **10**, 6019–6028.
- Guilderson T. P., Schrag D. P., Druffel E. R. M., Reimer R. W. (2021) Postbomb Subtropical
- North Pacific Surface Water Radiocarbon History. Journal of Geophysical Research:
- *Oceans* **126**, e2020JC016881.
- Heaton T. J., Köhler P., Butzin M., Bard E., Reimer R. W., Austin W.E.N., Bronk Ramsey C.,
- Grootes P.M., Hughen K. A., Kromer B., Reimer P. J., Adkins J., Burke A., Cook M. S.,
- Olsen J., Skinner L. C. (2020) Marine20 The Marine Radiocarbon Age Calibration
- 865 Curve (0-55,000 cal BP). *Radiocarbon* **62**, 779–820.
- 866 Hendy J. (2021) Ancient protein analysis in archaeology. Science Advances,
- 867 10.1126/sciadv.abb9314.
- Hill T. M., Myrvold C. R., Spero H. J., and Guilderson T. P. (2014) Evidence for benthic-pelagic
- food web coupling and carbon export from California margin bamboo coral archives.
- 870 *Biogeosciences* 11, 3845–3854.
- Holl S. M., Schaefer J., Goldberg W. M., Kramer K. J., Morgan T. D., and Hopkins T. L. (1992)
- 872 Comparison of Black Coral Skeleton and Insect Cuticle by combination of Carbon-13
- NMR and Chemical Analyses. *Archives of Biochemistry and Biophysics*, **292**, 107-111.

- 874 Ingalls A. E., Lee C., and Druffel E. R. M. (2003) Preservation of organic matter in mound-
- forming coral skeletons. *Geochimica et Cosmochimica Acta* **67**, 2827–2841.
- 876 Kaiser K. and Benner R. (2009) Biochemical composition and size distribution of organic matter
- at the Pacific and Atlantic time-series stations. *Marine Chemistry* **113**, 63-77.
- 878 Krull E. S., Baldock J. A., and Skjemstad J.O. (2003) Importance of mechanisms and processes
- of the stabilization of soil organic matter for modelling carbon turnover. *Functional Plant*
- 880 *Biology* **30**, 207–222.
- 881 LaRowe D. E. and Van Cappellen P. (2011) Degradation of natural organic matter: A
- thermodynamic analysis. *Geochimica et Cosmochimica Acta* **75**, 2030-2042.
- Larsen T., Ventura M., Andersen N., O'Brien D. M., Piatkowski U., and McCarthy, M. D.
- 884 (2013). Tracing carbon sources through aquatic and terrestrial food webs using amino
- acid stable isotope fingerprinting. *PloS one* **8**, e73441.
- Le Campion Alsumard T., Golubic S., and Hutchings P. (1995) Microbial endoliths in skeletons
- of live and dead corals: Porites lobata (Moorea, French Polynesia). *Marine Ecology*
- 888 *Progress Series* **117**, 149–158.
- Lehmann M. F., Bernasconi S. M., Barbieri A., and McKenzie J. A. (2002) Preservation of
- organic matter and alteration of its carbon and nitrogen isotope composition during
- simulated and in situ early sedimentary diagenesis. Geochimica et Cosmochimica Acta
- **66**, 3573–3584.
- 893 Catão A. J. L. and López-Castillo A. (2018) On the degradation pathway of glyphosate and
- glycine. Environmental Science: Processes and Impacts 20, 1148-1157.

895 McCarthy M. D., Benner R., Lee C. and Fogel M. L. (2007) Amino acid nitrogen isotopic 896 fractionation patterns as indicators of heterotrophy in plankton, particulate, and dissolved 897 organic matter. Geochimica et Cosmochimica Acta 71, 4727–4744. 898 McCarthy M. D., Lehman J., and Kudela R. (2013) Compound-specific amino acid δ^{15} N patterns 899 in marine algae: Tracer potential for cyanobacterial vs. eukaryotic organic nitrogen 900 sources in the ocean. Geochimica et Cosmochimica Acta 103, 104-120. 901 McMahon K. W., Fogel M. L., Elsdon T. S., and Thorrold, S. R. (2010). Carbon isotope 902 fractionation of amino acids in fish muscle reflects biosynthesis and isotopic routing from 903 dietary protein. Journal of Animal Ecology 79, 1132-1141. 904 McMahon K. W., McCarthy M. D., Sherwood O. A., Larsen T., and Guilderson T. P. (2015) 905 Millennial-scale plankton regime shifts in the subtropical North Pacific Ocean. Science 906 **350**, 1530–1533. 907 McMahon K. W. and McCarthy M. D. (2016) Embracing variability in amino acid δ¹⁵N 908 fractionation: Mechanisms, implications, and applications for trophic ecology. *Ecosphere* 909 7, 1–26. 910 McMahon K. W., Williams B., Guilderson T. P., Glynn D. S., and McCarthy M. D. (2018) Calibrating amino acid δ^{13} C and δ^{15} N offsets between polyp and protein skeleton to 911 912 develop proteinaceous deep-sea corals as paleoceanographic archives. Geochimica et 913 Cosmochimica Acta 220, 261-275. 914 Nielsen J. M., Popp B. N., and Winder M. (2015). Meta-analysis of amino acid stable nitrogen 915 isotope ratios for estimating trophic position in marine organisms. Oecologia 178, 631-916 642.

917 Noé S. U. and Dullo W. C. (2006). Skeletal morphogenesis and growth mode of modern and 918 fossil deep-water isidid gorgonians (Octocorallia) in the West Pacific (New Zealand and 919 Sea of Okhotsk). Coral reefs, 25, 303-320. 920 Noé S., Lembke-Jene L., Reveillaud J., and Freiwald A. (2007). Microstructure, growth banding 921 and age determination of a primnoid gorgonian skeleton (Octocorallia) from the late 922 Younger Dryas to earliest Holocene of the Bay of Biscay. Facies, 53, 177-188. 923 Ohkouchi N., Chikaraishi Y., Close H. G., Fry B., Larsen T., Madigan D. J., McCarthy M. D., 924 McMahon K. W., Nagata T., Naito Y. I., Ogawa N. O., Popp B. N., Steffan S., Takano 925 Y., Tayasu I., Wyatt A. S. J., Yamaguchi Y. T., and Yokoyama Y. (2017) Advances in 926 the application of amino acid nitrogen isotopic analysis in ecological and biogeochemical 927 studies. Organic Geochemistry 113, 150-174. Quay P., Sonnerup R., Westby T., Stutsman J., McNichol A. (2003) Changes in the ¹³C/¹²C of 928 929 dissolved inorganic carbon in the ocean as a tracer of anthropogenic CO₂ uptake. Global 930 Biogeochemical Cycles 17, 1004. 931 Ramirez M. D., Besser A. C., Newsome S. D., and McMahon K. W. (2021) Meta-analysis of 932 primary producer amino acid δ15N values and the ir influence on trophic position 933 estimation. *Methods Ecol Evol.* **12**, 1750–1767. 934 Roark E. B., Guilderson T. P., Dunbar R. B., and Ingram B. L. (2006) Radiocarbon-based ages 935 and growth rates of Hawaiian deep-sea corals. Marine Ecology Progress Series 327, 1-936 14. 937 Romanek C. S., Grossman E. L., and Morse J.W. (1992) Carbon isotopic fractionation in 938 synthetic aragonite and calcite: Effects of temperature and precipitation rate. Geochimica

et Cosmochimica Acta 113, 150-174.

940 Saino T. and Hattori A. (1980) ¹⁵N natural abundance in oceanic suspended particulate matter. 941 *Nature* **283**, 752–754. 942 Saino T. and Hattori A. (1987) Geographical variation of the water column distribution of 943 suspended particulate organic nitrogen and its ¹⁵N natural abundance in the Pacific and its marginal seas. Deep Sea Research Part A, Oceanographic Research Papers 34, 807–827. 944 945 Sauthoff W. (2016) Nitrogen Isotopes of Amino Acids in Marine Sediment: A Burgeoning Tool to Assess Organic Matter Quality and Changes in Supplied Nitrate ¹⁵N. University of 946 947 California Santa Cruz, Master's Thesis. 948 Schiff J. T., Batista F. C., Sherwood O. A., Guilderson T. P., Hill T. M., Ravelo A. C., McMahon 949 K. W. and McCarthy M. D. (2014) Compound specific amino acid δ^{13} C patterns in a 950 deep-sea proteinaceous coral: Implications for reconstructing detailed δ^{13} C records of 951 exported primary production. *Marine Chemistry* **166**, 82–91. 952 Shen Y., Guilderson T. P., Sherwood O. A., Castro C. G., Chavez F. P. and McCarthy M. D. (2021) Amino acid δ^{13} C and δ^{15} N patterns from sediment trap time series and deep-sea 953 corals: Implications for biogeochemical and ecological reconstructions in paleoarchives. 954 955 Geochimica et Cosmochimica Acta 297, 288–307. 956 Sherwood O. A., Guilderson T. P., Batista F. C., Schiff J. T. and McCarthy M.D. (2014) 957 Increasing subtropical North Pacific Ocean nitrogen fixation since the Little Ice Age. 958 *Nature* **505**, 78–81. 959 Sherwood O. A. and Edinger E. N. (2009) Ages and growth rates of some deep-sea gorgonian 960 and antipatharian corals of Newfoundland and Labrador. Canadian Journal of Fisheries 961 and Aquatic Sciences 66, 142-152.

- 962 Sherwood O. A., Lehmann M. F., Schubert C. J., Scott D. B. and McCarthy M. D. (2011) 963 Nutrient regime shift in the western North Atlantic indicated by compound-specific $\delta^{15}N$ 964 of deep-sea gorgonian corals. Proceedings of the National Academy of Sciences of the 965 United States of America 108, 1011–1015. 966 Sherwood O. A., Scott D. B. and Risk M. J. (2006) Late Holocene radiocarbon and aspartic acid 967 racemization dating of deep-sea octocorals. Geochimica et Cosmochimica Acta 70, 2806– 2814. 968 969 Sherwood O. A., Thresher R. E., Fallon S. J., Davies D. M. and Trull T.W. (2009) Multi-century time-series of ¹⁵N and ¹⁴C in bamboo corals from deep Tasmanian seamounts: Evidence 970 971 for stable oceanographic conditions. *Marine Ecology Progress Series* **397**, 209–218. 972 Silfer J. A., Engel M. H., Macko S. A. and Jumeau E. J. (1991) Stable carbon isotope analysis of 973 amino acid enantiomers by conventional isotope ratio mass spectrometry and combined 974 gas chromatography/isotope ratio mass spectrometry. Analytical Chemistry 63, 370–374. 975 Strzepek K. M., Thresher R. E., Revill A. T., Smith C. I., Komugabe A. F. and Fallon S. F. 976 (2014) Preservation effects on the isotopic and elemental composition of skeletal 977 structures in the deep-sea bamboo coral Lepidisis spp. (Isididae). Deep-Sea Research 978 Part II: Topical Studies in Oceanography 99, 199–206. 979 Stuiver M., Reimer P.J. and Reimer R. W. (2021) CALIB 8.2 http://calib.org (accessed Feb-7-980 2021). 981 Sun X. and Turchyn A. V. (2014) Significant contribution of authigenic carbonate to marine
- Tesdal J. E., Galbraith E. D. and Kienast M. (2013) Nitrogen isotopes in bulk marine sediment:
 Linking seafloor observations with subseafloor records. *Biogeosciences* 10, 101–118.

carbon burial. *Nature Geoscience* **8**, 1–4.

| 985 | Williams B. (2020). Proteinaceous corals as proxy archives of paleo-environmental change. |
|-----|---|
| 986 | Earth-Science Reviews 209, 103326. |
| 987 | Williams B. and Grottoli A. G. (2010) Recent shoaling of the nutricline and thermocline in the |
| 988 | western tropical Pacific. Geophysical Research Letters 37, 2-6. |
| 989 | Yamashita Y. and Tanoue E. (2003) Distribution and alteration of amino acids in bulk DOM |
| 990 | along a transect from bay to oceanic waters. Marine Chemistry 82, 145-160. |
| 991 | Zaiontz C. (2019) Real Statistics Resource Pack software (Release 6.2). Copyright (2013 – 2019) |
| 992 | www.real-statistics.com |
| 993 | |

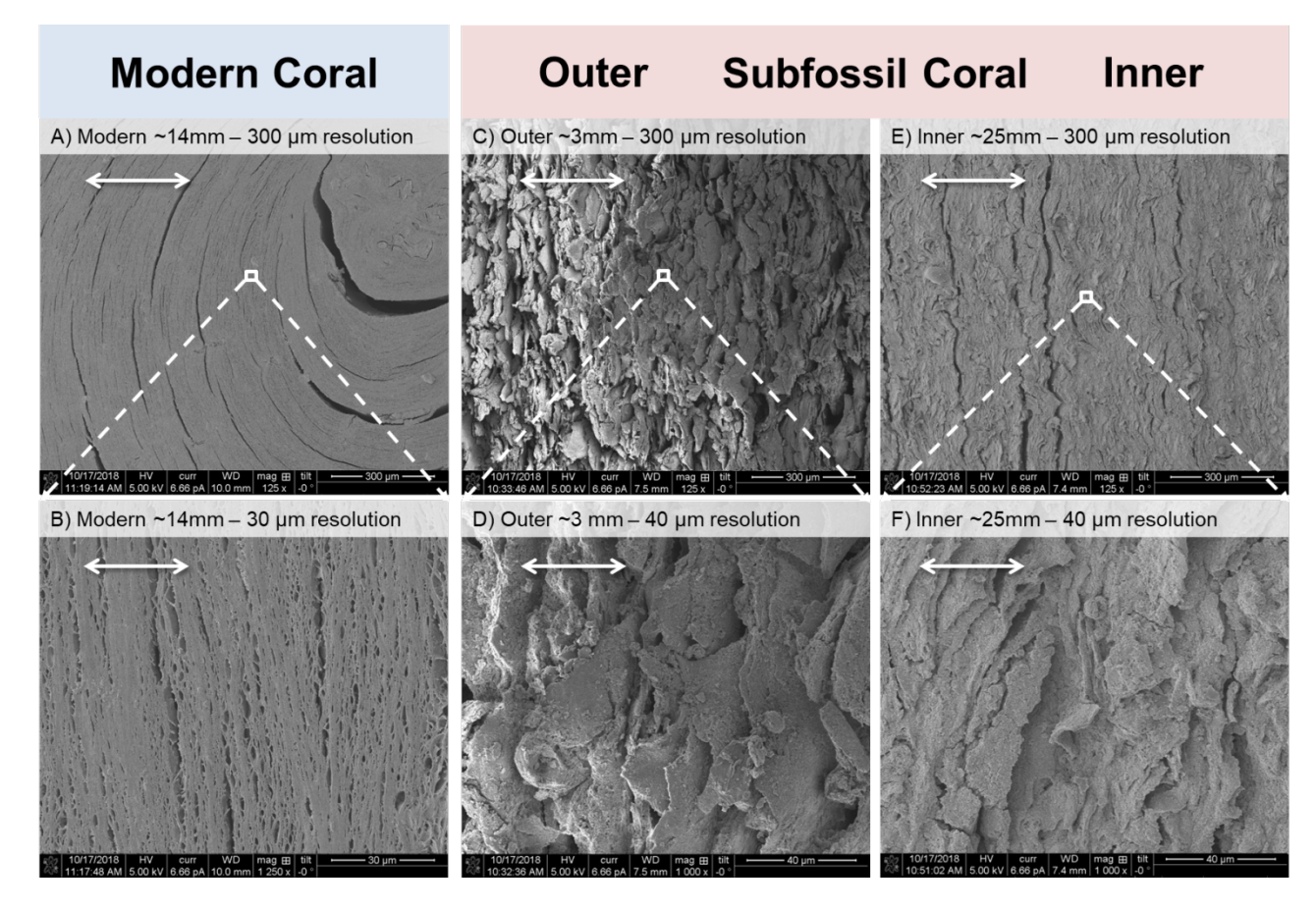


Fig. 1) Scanning electron microscope (SEM) images live-collected *Kulumanamana haumaaea* and subfossil gold coral skeletons collected from the same Cross Seamount location. For all figures, the growth axis progresses from right to left (outer layers left, inner layers right). Images on the top are magnified by 125x while the bottom are higher magnifications and representing the area inside the red squares on top images; scale bars are white arrows and also on lower right of each image. **A and B)** Live-collected coral skeletons showing the layered fibrous nature of living skeletons from ~14 mm from edge. Panel B is a 1250x (30 μm) magnified image of the modern of area in the white square; ~600 yr CE). **C and D)** Outer subfossil coral material, ~3 mm from the outer edge (~9.6 kyrs BP), which shows extreme structural alteration at 1000x (40 μm) magnification. **E and F)** Inner subfossil coral material imaged ~25 mm from the edge (~10.7 kyr BP), with similar magnifications to the outer layers.

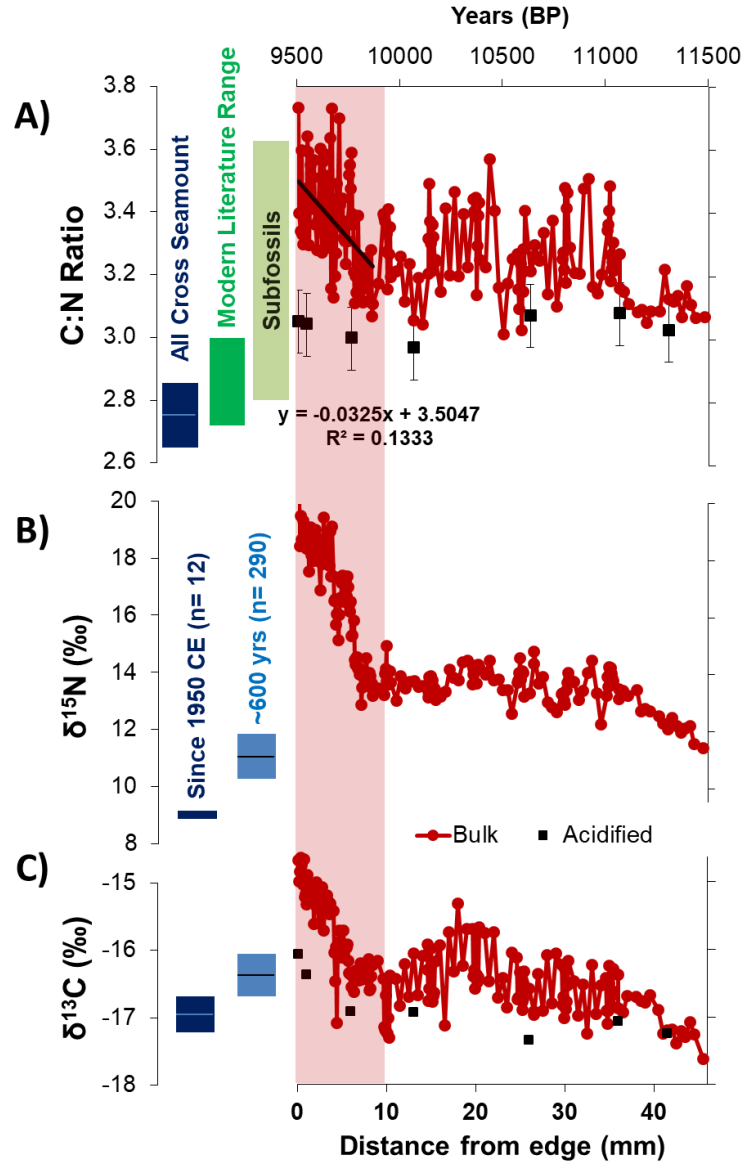


Fig. 2) C/N and bulk isotope values. **A)** C/N ratios for *K. haumaeea* coral skeletons. From left to right, a live-collected Cross Seamount coral C/N average and standard deviation (blue, this study), literature range for live-collected corals (dark green; Druffel et al., 1995, Goodfriend 1997; Sherwood et al., 2014; McMahon et al., 2015), range of previous dead-collected, subfossil coral values (light green; 1-5 kyrs BP, Glynn et al., 2019), and this study's results for a subfossil Cross Seamount skeleton (red). **B)** Bulk nitrogen and **C)** bulk carbon isotope values of live-collected (blue boxes) and subfossil *K. haumaeea* (red) gorgonin skeletal material, collected from the same Cross Seamount site. Due to the rapid change in isotopic values during the Industrial Revolution, live-collected coral values are plotted as separate averages and standard deviations for recent time (dark blue, since 1950 CE) versus the pre-Industrial Revolution (before 1900 CE, ~600 yrs). The subfossil coral data represents a 46 mm transect from the outer layers to the inner layers, with each point representing 0.1 mm resolution (~5-7 yrs). Black

squares are for selected acidified samples. Pink shading represents the outer 10 mm diagenetic horizon discussed in the text.

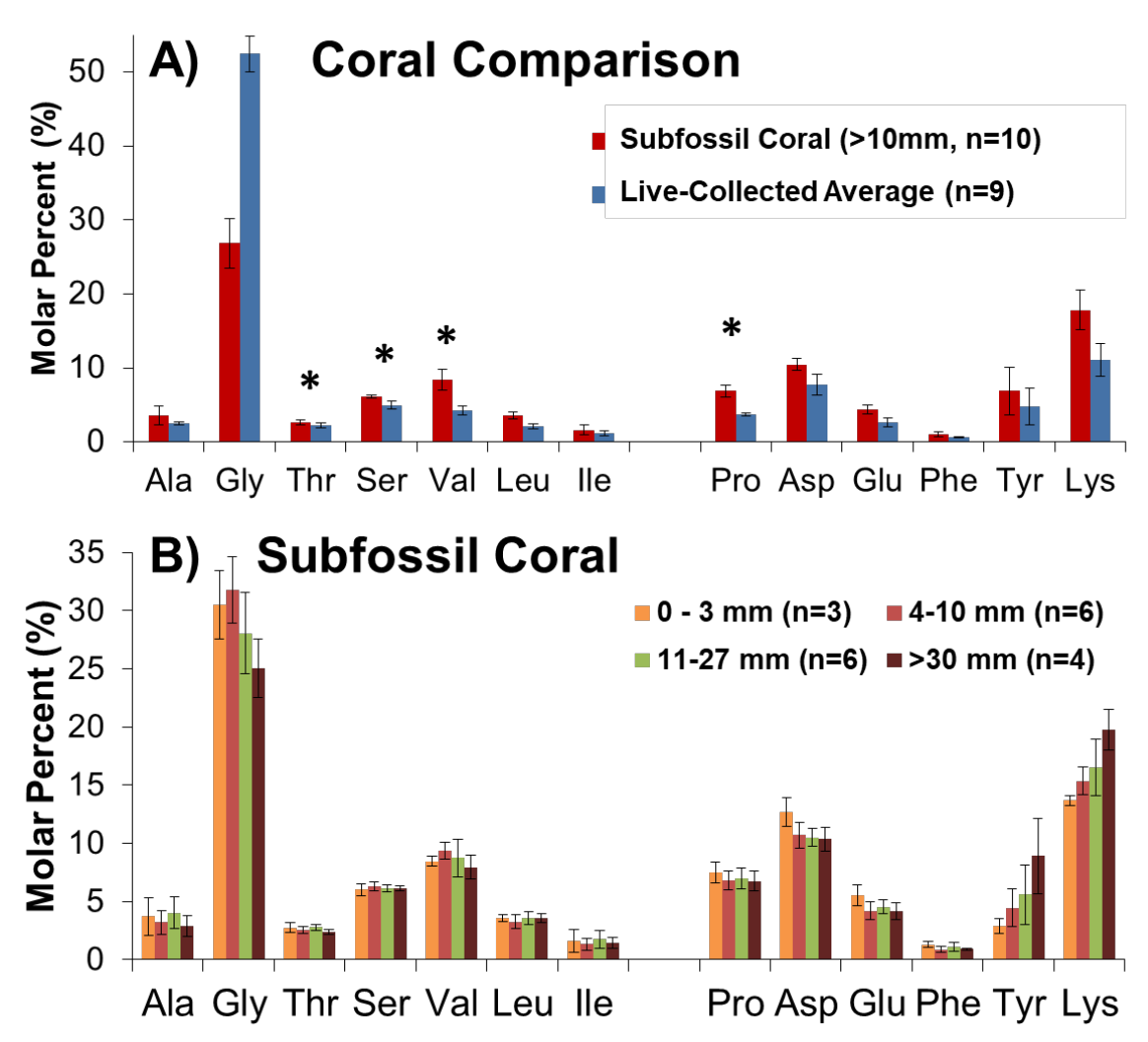


Fig. 3) Molar percentage (mol%_{AA}) of AAs for ancient and modern *K. haumaeea* skeletons. **A**) Subfossil vs. Modern *K. haumaeea* mol%_{AA} comparison. Average molar distribution in modern specimen (n=9; blue bars) versus average of only subfossil coral inner layers (>10 mm, n=10, red bars). There were significant mol%_{AA} differences between all AAs (P <0.02) except Tyr (P <0.12) and Ile (P <0.09; t-test assuming unequal variances, alpha = 0.05). AA's denoted with a star (*) indicate AA's which retain significantly different mol%_{AA} values if Gly values are set to be equal, as described in the text. **B**) Inter-coral subfossil skeleton mol%_{AA} data (n=19) from Cross Seamount, HI. Data are binned by skeletal depth highlighting AA composition changes between degraded outer layers vs. protected inner layers.

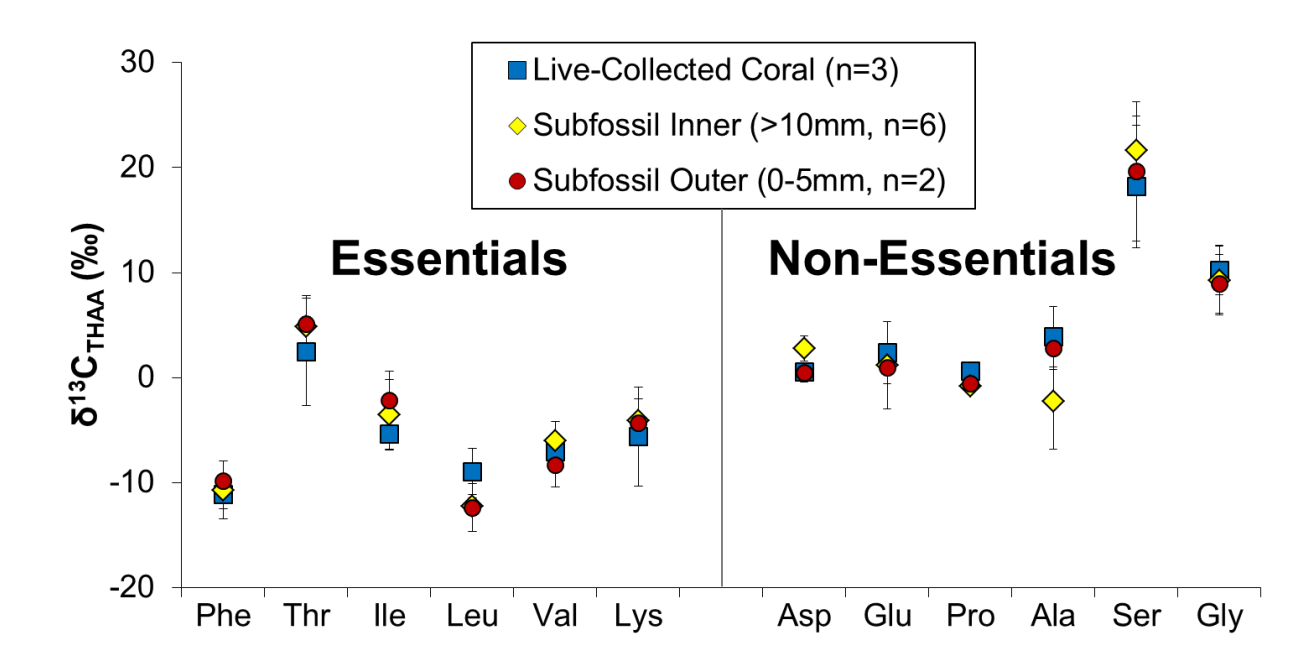


Fig. 4) Normalized δ^{13} C AA values in live-collected (blue) and subfossil *K. haumaeea* skeletons (red and yellow). AA δ^{13} C values normalized by subtraction of average THAA (δ^{13} C_{THAA}). AAs are grouped as described in the text and error bars indicate the standard deviation of the average binned δ^{13} C values.



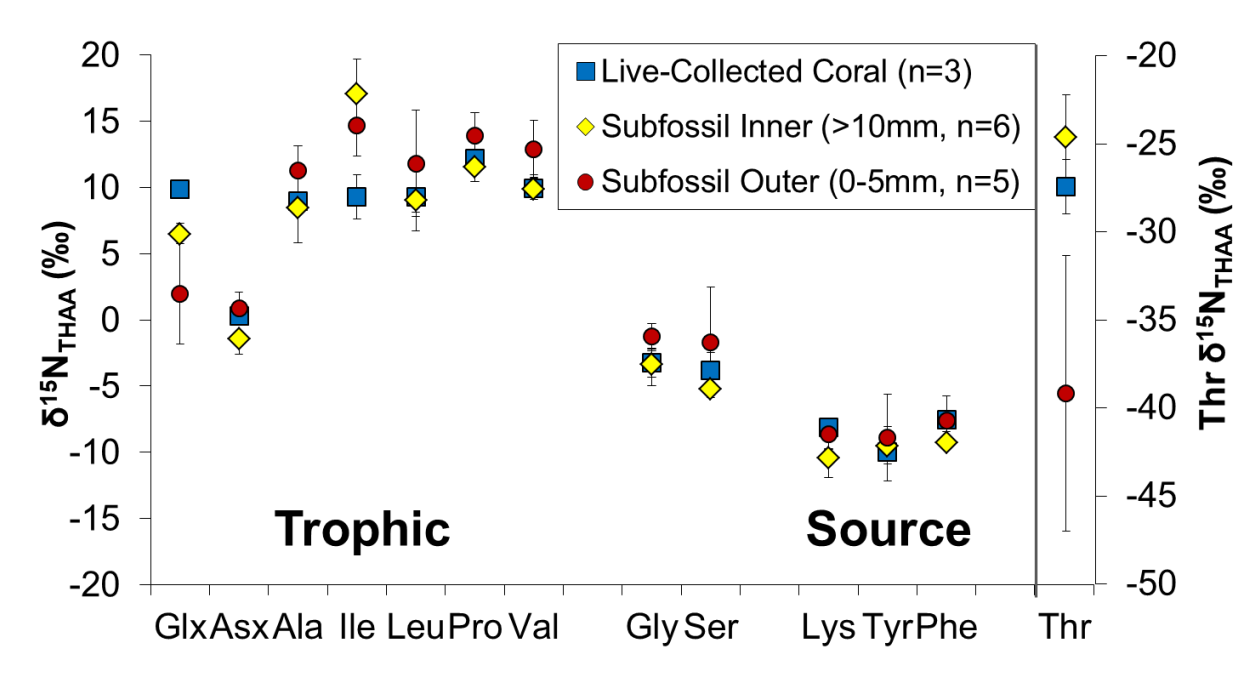


Fig. 5) Normalized δ^{15} N isotope values for AAs of the live-collected (blue) and subfossil K. *haumaeea* skeletons (red and yellow). AA δ^{15} N values normalized by subtraction to average δ^{15} N of hydrolysable protein (THAA parameter; see methods). Note that Thr is plotted on a separate secondary axis. AAs are grouped as described in the text and error bars indicate the standard deviation of the binned coral values.

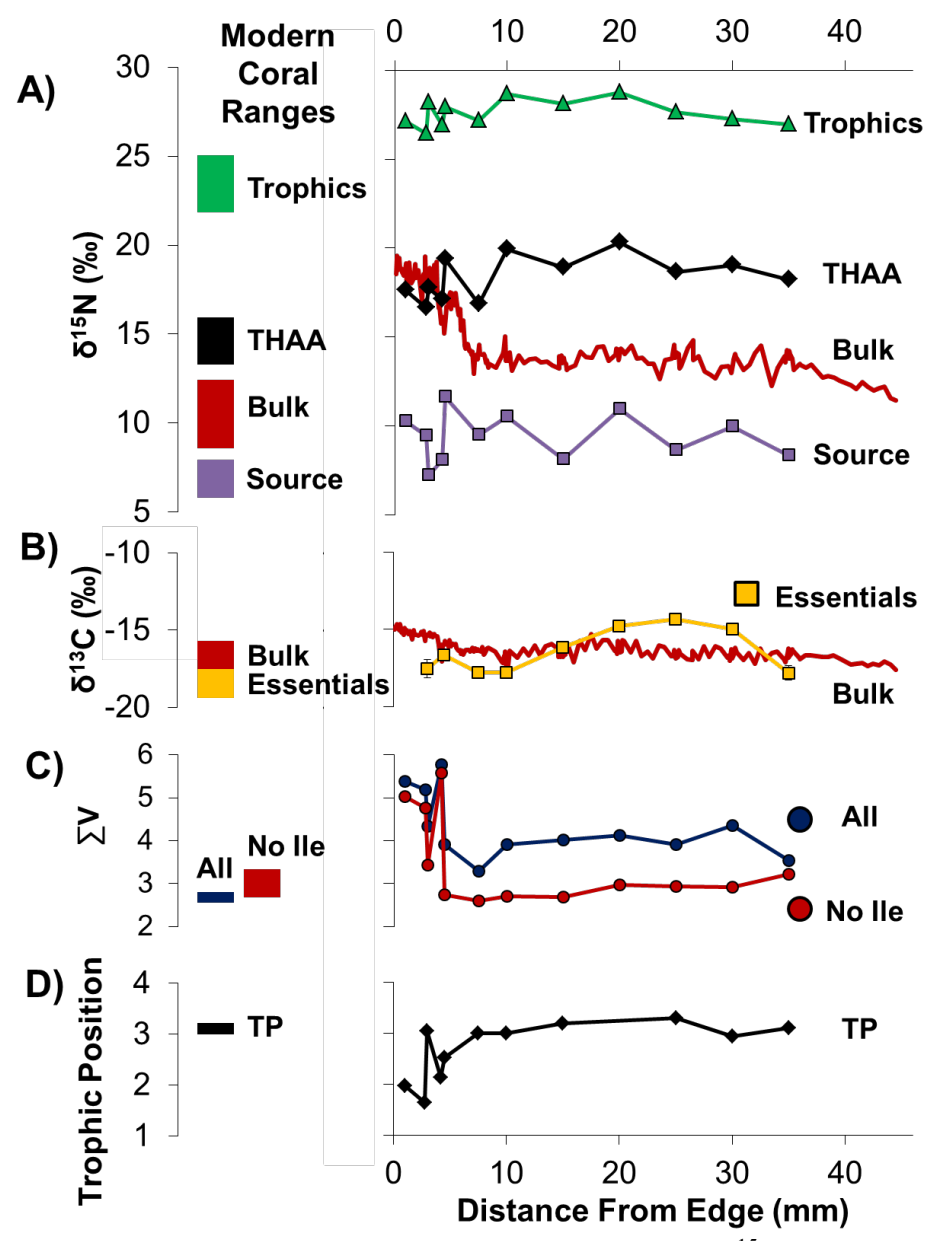


Fig. 6) Modern coral ranges compared to subfossil coral $\delta^{15}N_{AA}$ proxies. Ranges of values found for the modern specimen on the left and the subfossil coral on the right. **A)** Bulk $\delta^{15}N$ values plotted along with average total hydrolysable AAs (THAA) $\delta^{15}N$ average values (black), average $\delta^{15}N$ value of the trophic AAs (Glx, Asx, Ala, Ile, Leu, Pro, Val), and average $\delta^{15}N$ values source AA values (Phe, Lys, Tyr). **B)** Average of measured $\delta^{13}C$ values for essential AA (Phe, Thr, Ile, Leu, Val, Lys) plotted along with the bulk $\delta^{13}C$ values. **C)** ΣV values, calculated using all trophic AAs (blue) and excluding Ile values (red). **D)** Trophic position after McMahon et al. 2018 (see methods).